Typeset using LaTeX default style in AASTeX631

Draft version October 15, 2024

The Tale of Two Telescopes: How Hubble Uniquely Complements the James Webb Space Telescope: Galaxies

Rogier A. Windhorst,[1] Jake Summers,[1] Timothy Carleton,[1] Seth H. Cohen,[1] Kevin S. Croker,[1,2] Rolf A. Jansen,[1] Rosalia O'Brien,[1] Brent M. Smith,[1] Christopher J. Conselice,[3] Jose M. Diego,[4] Simon P. Driver,[5] Brenda Frye,[6] Benne W. Holwerda,[7] and Haojing Yan[8]

[1]*School of Earth and Space Exploration, Arizona State University, Tempe, AZ 85287-6004, USA*

[2]*Department of Physics and Astronomy, University of Hawai'i at Mānoa, 2505 Correa Rd., Honolulu, HI, 96822*

[3]*Jodrell Bank Centre for Astrophysics, Alan Turing Building, University of Manchester, Oxford Road, Manchester M13 9PL, UK*

[4]*Instituto de Física de Cantabria (CSIC-UC). Avenida. Los Castros s/n. 39005 Santander, Spain*

[5]*International Centre for Radio Astronomy Research (ICRAR) and the International Space Centre (ISC), The University of Western Australia, M468, 35 Stirling Highway, Crawley, WA 6009, Australia*

[6]*Steward Observatory, University of Arizona, 933 N Cherry Ave, Tucson, AZ, 85721-0009, USA*

[7]*Department of Physics and Astronomy, University of Louisville, Louisville KY 40292, USA*

[8]*Department of Physics and Astronomy, University of Missouri, Columbia, MO 65211, USA*

ABSTRACT

In this paper, we present a simple but compelling argument, focusing on galaxy science, for preserving the main imagers and operational modes of the Hubble Space Telescope (HST) for as long as is technically feasible. The James Webb Space Telescope (JWST), fully operational since summer 2022, was designed to explore the epochs of First Light, Galaxy Assembly, and Super Massive Black Hole (SMBH) growth, and has been doing so in spectacular detail at wavelengths 0.9–28 μm. HST was designed to work well in the 0.1–1.6 μm wavelength range. While its primary (and only original) goal was to measure the Hubble constant, H_0, to within 10%, it has done so today to within a few %. HST's unique UV–optical performance has fundamentally contributed to our understanding of Galaxy Assembly and the Cosmic Star Formation History (CSFH). While star-formation started at redshifts z$\gtrsim$10–13, when the universe was less than 300–500 Myr old, the CSFH did not peak until z$\simeq$1.9 (i.e., about 10 Gyr ago), and has steadily declined since that time. Hence, at least half of all stars in the universe formed in the era where HST provides its **unique rest-frame UV view of unobscured young, massive stars tracing cosmic star-formation.** By rendering a subset of the 556.3 hours of available HST images in 12 filters of the Hubble Ultra Deep Field (HUDF) in an appropriate mix of colors, we illustrate the unique capabilities of HST for galaxy science emphasizing that rest-frame UV–optical wavelength range. We then contrast this with the 52.7 publicly available hours of JWST/NIRCam images in 8 filters of the same HUDF area from the JADES project, rendering these at the redder near-IR wavelengths to illustrate the unique capabilities of JWST to detect older stellar populations at higher redshifts, as well as very dusty stellar populations and Active Galactic Nuclei (AGN). [a)] HST uniquely probes (unobscured) young, hot, massive stars in galaxies, while JWST reveals more advanced stages of older stellar populations, as well as relatively short-lived phases where galaxies produce and shed a lot of dust from intense star-formation, and the very high redshift universe (z $\gtrsim$10–11) not accessible by HST. **We conclude that HST and JWST are *highly complementary* facilities that took decades to build to ensure decades of operation. To maximize return on investment on both HST and JWST, ways will need to be found to operate HST imaging instruments in all relevant modes for as long as possible into the JWST mission.**

Keywords: Instruments: Hubble Space Telescope — Instruments: James Webb Space Telescope — Galaxies: Galaxy Assembly — Galaxies: Galaxy Counts — Cosmology: Extragalactic Background Light

Rogier.Windhorst@asu.edu

[a)] These HST+JWST PDF images may be too big for overleaf or astroph. Please view their full resolution PDF files on: http://www.asu.edu/clas/hst/www/jwst2024/ .

1. INTRODUCTION: BRIEF SYNOPSIS OF THE HUBBLE SPACE TELESCOPE AND THE THE JAMES WEBB SPACE TELESCOPE

The Hubble Space Telescope (HST) was designed in the 1960s and 1970s to observe very faint objects at UV to near-IR wavelengths above the Earth's atmosphere (*e.g.*, Smith et al. 1993). HST's ability to observe outside the Earth's atmosphere has resulted in very significant gains over ground-based telescopes in four main areas, namely the ability to: (1) observe in the vacuum ultraviolet; (2) observe with very stable, repeatable, and narrow Point-Spread Functions (PSFs); (3) observe against very dark foregrounds and backgrounds; and (4) perform precision (point-source) photometry at (very) high time-resolution, but also on timescales of minutes to decades. As of April 24, 2024, HST has been in orbit for over 34 years. After successful correction of the spherical aberration in its primary mirror in December 1993, HST has produced an unprecedented wealth of high-quality data that has fundamentally changed our understanding of the Universe, and of Galaxy Assembly and Super Massive Black Hole (SMBH) growth in particular. The HST Archive [1] presently contains over 2 million exposures from both its imagers and spectrographs.

Over the last 31 years, NASA's Hubble Space Telescope has become arguably the most successful science mission ever undertaken. From the STScI EPO office, we obtained the following data to support this bold statement. NASA's Hubble Space Telescope (HST) had ∼1200 science press releases since 1990, each with ≳400 million readers (or impressions) worldwide. That is, approximately $\sim 480 \times 10^9$ reads (or impressions) of Hubble press releases in total. At about 8×10^9 humans on Earth currently (assuming ages somewhat larger than HST's), thus *on average* each human would have read ≳60 Hubble stories, and some smaller fraction would have read many more during their lifetimes. HST is *the most publicized* space astrophysics mission in NASA history. HST has yielded on average ≳500–1300 refereed papers/year by the astronomical community since 1990, counting ≳46,000 HST papers on ADS currently (with "HST" in the paper abstracts), and ≳929,000 citations since 1990. As an observatory, the Hirsch index of the Hubble Space Telescope is then $h_{HST} \simeq 316$! HST continues to be productive even now with 1435 HST papers featured in 2023, more than Keck and ALMA combined. We will argue in this paper that it is too soon to dismantle HST and turn off some of its most productive instruments and operational modes.

The James Webb Space Telescope ("JWST") was designed in the 1990s and 2000s to observe very faint objects at near- and mid-infrared wavelengths from the Sun–Earth L2 Lagrange point (*e.g.*, Rieke et al. 2005; Gardner et al. 2006; Beichman et al. 2012; Windhorst et al. 2008; Gardner et al. 2023; Rieke et al. 2023b; Windhorst et al. 2023). With its 6.5-meter aperture and state-of-the-art scientific instruments,[2] JWST builds on the scientific results from two of NASA's previous flagship missions: the Hubble Space Telescope (HST; for a review of 27 years of HST imaging data, see, *e.g.*, Windhorst et al. 2022), and the Spitzer Space Telescope (see, *e.g.*, Werner et al. 2004; Soifer et al. 2008; Werner et al. 2022).

2. WHAT HST HAS DONE ON GALAXIES IN THE LAST THREE DECADES THAT SET THE STAGE FOR JWST

Here, we present a simple but compelling argument, focusing on galaxy science, for preserving the main imagers and operational modes of the Hubble Space Telescope (HST) for as long as is technically feasible. We were asked to focus on HST's galaxy science. The James Webb Space Telescope (JWST), operational since July 2022, was designed — amongst others — to explore the epochs of First Light, Galaxy Assembly, and Super Massive Black Hole growth, and started to do so in spectacular detail at wavelengths 0.9–28 μm. HST was designed to work well in the 0.1–1.6 μm wavelength range. While its primary (and only original) goal was to measure the Hubble constant, H_0, to within 10%, it has done so today to within a few % (*e.g.*, Freedman & Madore 2023; Riess et al. 2024; Freedman et al. 2024). However, the Hubble Space Telescope has had a far wider impact than measuring the expansion rate alone.

The topic of of Galaxy Assembly has been one of the main areas where HST has made very significant breakthroughs due to its superb spatial resolution and its very stable dark sky-values. The number of HST papers on Galaxy Assembly has been too numerous to review here, but we will mention some of the main deep field work done with HST. Hubble's first Deep Field was the HDF for a total of 150 orbits in HST's Continuous Viewing Zone (CVZ) (Williams et al. 1996), which was inspired amongst others by earlier medium-deep field work with the refurbished telescope since

[1] https://archive.stsci.edu

[2] https://www.stsci.edu/jwst/ and https://www.stsci.edu/jwst/instrumentation/

1994: amongst these were, *e.g.*, the 32 orbit WFPC2 image of the radio galaxy 3C324 and its environment at z=1.21 (Dickinson et al. 1995; Dickinson 1995), the 67 orbit WFPC2 images of the protocluster around the radio galaxy 53W002 at z=2.39 (Pascarelle et al. 1996a,b), and the HST Medium Deep Survey done with WFPC2 in parallel mode (*e.g.*, Griffiths et al. 1994; Driver et al. 1995). The HDF and its precursors showed that galaxy assembly started from smaller sub-galactic clumps that over cosmic time grew into the well known elliptical and spiral galaxies that we observe today (*e.g.*, Driver et al. 1998, and references therein). The HDF was followed-up in the near-IR with the NICMOS camera after it was installed into Hubble in 1997 (Thompson et al. 1999), which started to show the first, more mature galaxies with older stellar populations at higher redshifts. The HDF observations with WFPC2 and NICMOS and their resulting papers were such a remarkable success that, as soon as the ACS was installed in March 2002, a campaign was planned for the Hubble UltraDeep Field (HUDF) and its surrounding GOODS-South area, and was carried out in 2003–2004 (*e.g.*, Beckwith et al. 2006; Giavalisco et al. 2004, and references therein). After the successful installation of the WFC3 in May 2009, the HUDF, GOODS-South and other fields were followed-up in the UV and near-IR, resulting in surveys like the WFC3 ERS (*e.g.*, Windhorst et al. 2011), the UV-UDF (*e.g.*, Teplitz et al. 2013; Rafelski et al. 2015), the HDUV (*e.g.*, Oesch et al. 2018), the UDF12 (Koekemoer et al. 2013) and the XDF (*e.g.*, Illingworth et al. 2013, and references therein). To help average over the effects of cosmic variance these surveys were expanded over more and larger areas through surveys like CANDELS (*e.g.*, Grogin et al. 2011; Koekemoer et al. 2011) and COSMOS (*e.g.*, Scoville et al. 2007; Kartaltepe et al. 2007, and references therein).

In summary, during the last three decades, these four refurbished instruments of HST showed that the process of galaxy assembly started at high redshifts from small actively starforming objects growing and merging into the large and luminous elliptical and spiral galaxies that we see today. HST has shown that the galaxy merger rate was higher in the past, with galaxy growth taking place both through mergers and through in-situ star formation (*e.g.*, Duncan et al. 2019). HST's unique UV–optical performance has thus spectacularly contributed to our understanding of Galaxy Assembly and the Cosmic Star Formation History (CSFH). We now know that cosmic star-formation started at redshifts $z \gtrsim 10$–13 when the universe was less than 300–500 Myr old, but that the CSFH did not peak until $z \simeq 1.9$ (i.e., about 10 Gyr ago; Madau & Dickinson 2014, see Fig. 1 here) and has steadily declined since that time (*e.g.*, Lilly et al. 1996). Fig. 1 shows that approximately the same is also true for AGN accretion disks around SMBHs, as these grew over cosmic time approximately in sync with galaxy bulge growth (*e.g.*, Magorrian et al. 1998; Gebhardt et al. 2000; Kormendy & Ho 2013), implying that AGN feedback played a critical role in massive galaxy assembly.

Throughout, we will use the fact that unobscured young hot stars — and unobscured AGN accretion disks — will have their rest-frame UV-light shine through the neutral hydrogen in the Inter Galactic Medium (IGM) at wavelengths $\lambda \gtrsim 1216$ Å, and at lower redshifts down to 912 Å. Hence, the rest-frame UV light from these sources — which have typical effective temperatures T$\gtrsim$10,000–30,000 K — will span the wavelength range of ∼1216–3000 Å, which at $z \lesssim 2$ is the sole domain of HST's unique capabilities over its observable wavelength range of ∼2000–9000Å for wide-field near-UV–optical imaging. **In conclusion, Fig. 1 shows that at least half of all stars in the universe formed in the era where HST provides its unique rest-frame UV view of unobscured young, massive stars that trace star-formation, as well as of AGN accretion disks around growing super-massive black holes.** Fig. 2 shows the throughput curves of the HST (blue) and JWST (red) filters, to illustrate how these were used in § 3 to render the full complement of available HUDF data, with a star-forming (blue) and old (red) elliptical galaxy SED overlaid at the peak redshift $z \simeq 1.9$ of the cosmic SFH. **Both HST and JWST sample essential and very complementary phases of galaxy assembly that thus must continue to be studied with both telescopes!**

3. WHY HST IS FUNDAMENTALLY COMPLEMENTARY TO JWST AND MUST NOT BE DISMANTLED

By rendering a subset of the 556.3 hours of available HST images in 12 filters of the Hubble Ultra Deep Field (HUDF; Beckwith et al. 2006; Teplitz et al. 2013; Rafelski et al. 2015) in an appropriate mix of colors following the prescriptions of Windhorst et al. (2011) and Coe (2015), we illustrate the unique capabilities of HST for galaxy science emphasizing the rest-frame UV–optical wavelength range. We then contrast this with the 52.7 hours of publicly available JWST/NIRCam images in 8 filters of the same HUDF area from the JADES project (*e.g.*, Rieke et al. 2023a; Eisenstein et al. 2023), where we multiplied the actual JWST observing hours by 2 to represent the total exposure time in each of the simultaneously-exposed NIRCam SW and LW filter pairs. We render these NIRCam filters in redder colors to visually illustrate JWST's unique near-IR capabilities to detect older stellar populations at higher redshifts, as well as very dusty stellar populations and Active Galactic Nuclei (AGN). HST uniquely probes (unobscured)

young, hot, massive stars in galaxies, while JWST reveals more advanced stages of older stellar populations, including relatively short-lived phases where galaxies produce and shed a lot of dust from intense star-formation, and the very rare high redshift objects (z$\gtrsim$10–13) not accessible by HST.

Panchromatic studies of the Integrated Galaxy Light (IGL; see also §4b) have shown that *approximately equal parts* of the energy from cosmic star-formation plus cosmic AGN growth comes from these populations that are: a) largely unobscured by dust in the rest-frame UV-optical; and b) significantly obscured by dust in the rest-frame UV-optical, and therefore best detected from near-IR to millimeter wavelengths (*e.g.*, Driver et al. 2016; Andrews et al. 2018; Koushan et al. 2021, and references therein). Hence, as we will detail below, **HST alone is as important to image these populations as facilities like, *e.g.*, JWST, Spitzer, WISE, Herschel and ALMA are combined.**

Cosmic star-formation often occurs in small clumps, which are completely unresolved from the ground and are still very small in HST images with median FWHM sizes $\lesssim$0.″2 to AB$\lesssim$27 mag (*e.g.*, Fig. 10a of Windhorst et al. 2011). Hence, they require HST's exquisite UV-optical imaging capabilities from space, which in well-dithered and drizzled images can have PSF FWHM values as narrow as 0.″05–0.″06. To confirm the high redshift candidates that JWST is now finding, and to and understand their nature, deep HST optical imaging is essential to reliably remove lower redshift contaminants (*e.g.*, Adams et al. 2024; Conselice et al. 2024). Combining HST optical images with JWST NIRCam images yields more robust photometric redshift solutions and reduces contamination significantly, even when the HST filters are just probing below the Lyman break in the rest-frame.

Fig. 3 shows a full color image of the Hubble UltraDeep Field with 891 orbits (556.3 hours or 2.003 Msec spread over 3043 independent exposures) of HST time in 12 HST filters (*e.g.*, Beckwith et al. 2006; Teplitz et al. 2013; Rafelski et al. 2015). In Fig. 3, the WFC3/UVIS F225W, F275W, and F336W and ACS/WFC F435 filters have been noise-weighted and rendered in the blue channel, the ACS/WFC F606W, F775W, F814W and F850LP filters were noise-weighted and rendered in green, while the WFC3/IR filters F105W, F125W, F140W, and F160W were noise-weighted and rendered in red. All full HUDF images in Fig. 3–6 are shown at 0.″06/pixel, and are 2580×2510 pixels (or 154.″8×150.″6) in size with North at a PA of +47.5° from vertical.

Fig. 4 shows a false color image of the Hubble UltraDeep Field in the 8 bluest HST filters (WFC3/UVIS F225W, F275W, and F336W and ACS/WFC F435W F606W, F775W, F814W and F850LP from Fig. 3), but now all noise-weighted and rendered **only in the blue channel**. This demonstrates the HST-unique UV–blue photons from *recent star-formation* at observed wavelengths $\lambda\lesssim$0.9 μm, that represent the more recent cosmic SFH at z$\simeq$0–2 — *i.e.*, from the peak in the cosmic SFH about 10 Gyrs ago and more recently, which JWST does not sample close to its diffraction limit at wavelengths at or below 0.8–1.0 μm (see also Fig. 5 here and Windhorst et al. 2023).

Fig. 5 shows a color image of the publicly available 52.7 hours JWST NIRCam JADES images (Rieke et al. 2023a; Eisenstein et al. 2023) of the same HUDF area covered by Hubble as in Fig. 3–4. To best illustrate the JWST sensitivity to infrared objects — and mimic the colors closest to what the human eye can see — all NIRCam filter images were noise-weighted and rendered in green (SW: F090W, F115W, F150W, F182M, F200W, and F210M) or in red (LW: F277W, F335M, F356W, F410M, and F444W). The JWST NIRCam data alone in Fig. 5 *sample the rest-frame optical part of the cosmic star-formation history at z$\lesssim$2*, and further into the rest-frame UV at z$\gtrsim$2 (see also Fig. 1 and 7e below). In Fig. 6, we will illustrate how HST provides the rest-frame UV for z$\lesssim$2, resulting in the full panchromatic suite of colors present in the entire cosmic star-formation history when compared to Fig. 5.

Fig. 6 shows a full color image of the *combined* public 361.3 hours HST + 52.7 hours JWST data of Fig. 4–5. Because the WFC3/IR images (195.0 hours spread over 1025 exposures) had lower spatial resolution and are not as deep as the 52.7 hours of JWST NIRCam images, these were omitted in this comparison, and only the 361.3 ACS/WFC+WFC3/UVIS hours (or 1.3007 Msec spread over 2018 independent exposures) that covered the *HST-unique* wavelengths of 0.2–0.9 μm were used. Note hat the ratio of available exposure times of a factor of 6.85 (HST/JWST = 361.3/52.7) is comparable to the aperture-area ratio of the two telescopes, so that in the small wavelength region of overlap (Fig. 2), the HST and JWST images reach comparable depths for isolated flat-spectrum point sources (see Fig. 7 for details). Hence, the comparison between the two telescopes that follows is as fair as we can make it with the current data. Next, the 8 bluest HST-unique filters (WFC3/UVIS F225W, F275W, and F336W and ACS/WFC F435W, F606W, F775W, F814W and F850LP) were noise-weighted and rendered in blue, the JWST NIRCam SW filter images were noise-weighted and rendered in green (F090W, F115W, F150W, F182M, F200W, and F210M), while the JWST NIRCam LW filter images were noise-weighted and rendered in red (F277W, F335M, F356W, F410M, and F444W). Note two unavoidable thin interchip-gaps cause a few objects to have unusual

purple colors. **At a total of 414.0 hours of combined telescope exposure time, this is to our knowledge the deepest available combined HST+JWST color image available from public data to date, and as we will see below, it demonstrates the very strong complementarity of HST to JWST.**

It is remarkable how the HST image-stack of the HUDF — rendered fully in blue in Fig. 6 using Fig. 4 — lifts out the more recent SF in galaxies at z$\lesssim$2, which tends to be often rather clumpy and sporadic, as well as the numerous faint blue dwarf galaxies in more recent cosmic epochs. The latter are the majority population for AB$\lesssim$27 mag (Driver et al. 1995, 1998), and probably also at fainter fluxes. It is also remarkable how well JWST — rendered for this purpose in green and red in Fig. 6 — lifts out the old stellar population in elliptical galaxies at z$\gtrsim$1 (the mostly green–orange objects), as well as the highly dust-obscured objects (mostly deep red but extended objects in Fig. 6), and the rare very high redshift objects at z$\gtrsim$10–13 (most faint brown–red colored point sources in Fig. 6). In addition, compared to HST, JWST also lifts out the weak central AGN, which are often seen as faint, very red or highly reddened objects that carry a clear point like central feature (*e.g.*, Ortiz et al. 2024). **In summary, HST unique UV–optical imaging capabilities adds the unobscured restframe UV+blue light that samples the more recent half of the CSFH in the last 10 billion years since z$\lesssim$2, when compared to the JWST restframe optical–near-IR light that samples the older and/or more dusty stellar populations, and the very few rare objects at z$\gtrsim$10–13 seen in the first 300–500 Myr.**

Fig. 7a–7d show an enlargement of an area from Fig. 6 containing several HUDF galaxies with a wide variety of morphologies and star-formation histories, illustrating the power of combining 361.3 hours of HST UV-optical images with 52.7 hours of JWST NIRCam images. The bottom panel Fig. 7e shows the throughput curves of the HST (in blue) and JWST (in green and red) filters reproduced from Fig. 2 once more for clarity, to illustrate how these were used to render the full complement of publicly available HUDF data in Fig. 3–7.

Fig. 8 shows a color image of the *combined public 122-hour HST Frontier Field images with ACS/WFC plus the 3-epoch 22-hour JWST PEARLS NIRCam images* on galaxy cluster MACS0416 at redshift z=0.397 (*e.g.*, Diego et al. 2023; Windhorst et al. 2023; Yan et al. 2023b)[3] . Like Fig. 6, this beautiful panchromatic MACS0416 image perfectly illustrates the power of combining HST images in the restframe UV–blue with JWST images in the restframe optical–near-IR. We conclude that HST is uniquely built to image the early (dust-unobscured) stages of hot massive star-formation in galaxies, while JWST is uniquely built to image the more advanced stages of older stellar populations in galaxies, as well as the phases where galaxies produce and shed a lot of dust from intense star-formation, and the very high redshift universe (z$\gtrsim$10–13) not accessible by HST. **In conclusion, HST and JWST are highly complementary facilities that took decades to build to ensure decades of operation. To maximize return on investment on both HST and JWST, ways will need to be found to operate HST unique UV–optical imaging instruments in their relevant modes for as long as possible into the JWST mission.**

4. RECENT RESULTS THAT USE ARCHIVAL OR NEW HST IMAGES, ESPECIALLY IN THE UV-OPTICAL

In this section, we will discuss recent results on "Galaxies" that use Archival or new HST images, especially in the UV-optical. STScI asked us to specifically write this section from the Galaxies perspective.

4.1. *Lyman Continuum Escape studies at z$\simeq$2–3.5 to find the main population(s) maintaining Cosmic Reionization*

It has long been uncertain what population(s) finished Cosmic Reionization by redshifts z$\simeq$6 — when the universe was only a billion years old — and which population(s) have maintained cosmic reionization for the 13 Gyrs since z$\simeq$6. It is only because the hydrogen in the IGM has remained on average ionized during the last 13 Gyrs that we can actually observe some of the redshifted rest-frame far-UV spectra ($\lambda\leq$1216 Å) of galaxies and quasars out to cosmological distances. Hydrogen reionization must be accomplished by rest-frame photons bluer than 912 Å (Lyman-continuum or LyC radiation), and so the logical astrophysical sources of LyC radiation are either hot stars — *i.e.*, those unobscured in the UV by surrounding neutral hydrogen clouds or dust — or accretion disks surrounding SMBHs. The suspected sources of cosmic reionization have traditionally been sought in either the population of dwarf galaxies, or those of quasars and weak AGN over cosmic time. In all cases, surrounding neutral hydrogen and dust has to be vacated before the LyC photons can become visible. For this reason, low-mass SF dwarf galaxies are plausible candidates, because

[3] This image was also featured on: https://www.nytimes.com/2023/12/19/science/christmas-stars-galaxies-webb-nasa.html?

supernovae (SNe) from their young stellar populations may produce enough holes in their Inter Stellar Medium (ISM) to enable their LyC radiation to escape. Similarly, quasars and even weak AGN may have produced sufficiently strong outflows driven by their inner SMBH accretion disks to produce (conical) paths along which LyC may have escaped. Massive galaxies are thought to be fainter LyC sources, because of their own significant dust production and because SN-driven outflows may not (or no longer) be sufficiently strong to push out the ambient hydrogen at escape velocity.

The experiment of where, when, and how LyC radiation can escape from these potential UV sources can be done in several ways. One is to directly measure spectroscopically with HST STIS or COS the escaping LyC radiation below 912 Å in the rest-frame, or via imaging with the STIS or ACS MAMA detectors of low redshift analogs. This is the topic of other papers (and chapters in the 2024 Senior Review), but beyond the scope of our current HST imaging assessment. We will focus here on the *most direct* way of measuring the LyC escape fraction at the redshifts where these photons are produced in bulk *and where they can in fact be measured*. With the UV-optimized CCDs in WFC3/UVIS, this limits us to redshifts $z \gtrsim 2.3$ using the F225W, F275W and F336W filters, and to redshifts $z \lesssim 3.5$ where the Lyman forest in the IGM becomes progressively more opaque, allowing for fewer clear lines-of-sights (LOS) at the higher redshifts to permit LyC radiation to travel through. Any estimates of the LyC escape fraction at higher redshifts must come from *indirect methods* using emission lines from spectra (*e.g.*, with JWST NIRSpec) and SED modeling of their stellar populations, which has its own uncertainties. This HST LyC work has been pioneered with WFC3/UVIS in the WFC3 ERS field (*e.g.*, Smith et al. 2018, 2020a), in the HDUV field (*e.g.*, Naidu et al. 2017; Oesch et al. 2018), and in the UVCANDELS survey (*e.g.*, Smith et al. 2024; Wang et al. 2023). In summary, the evidence available thus far suggests that weak AGN are more successful in producing escaping LyC radiation than dwarf galaxies on average (*e.g.*, Smith et al. 2020a, 2024), which is also supported by recent theoretical work (*e.g.*, Madau et al. 2024). **However, the currently available statistics on directly detected escaping LyC radiation remain small, and the measurements are difficult to accomplish, and so this work needs to continue for as long as possible with WFC3 UVIS in the rest-frame UV to complete the details of where, when and how LyC escapes.**

4.2. *Multi-Decade Monitoring of the Panchromatic HST Background to constrain Zodiacal Light models and Diffuse Light levels*

As summarized in § 1, most observers will use HST for its unique capabilities in the vacuum ultraviolet or at optical wavelengths, and/or to observe with its very stable, repeatable, and narrow PSFs against very dark foregrounds and backgrounds. What is often overlooked is that precisely the combination of HST's very dark sky surface brightness (sky-SB) environment *and* its ability to perform precision photometry on timescales of minutes to decades offers significantly new parameter space where unexpected discoveries can be made. At 0.8–1.6 μm wavelengths, the HST sky-SB in occultation is between ∼10–1000× darker than what can be obtained from the ground with broad-band observations. We have been asked to comment on these unique HST capabilities, and so will briefly summarize some of this work here. Since the launch of its refurbished cameras (WFPC2 in Dec. 1993, ACS in March 2002, and WFC3 in May 2009), over 1 million images have been taken with HST in the last 31 years, many but not all of fairly random areas of the sky. Details of this work — amongst others done through multi-year HST Archival Legacy project "SKYSURF" — can be found in Windhorst et al. (2022), who compiled approximately 249,000 independent HST exposures plus 891,000 WFC/IR on-the-ramp integrations to monitor the sky-SB values from Low Earth Orbit (LEO) in between the detected discrete objects, most of which, of course, are faint galaxies that make up the IGL, and Galactic stars.

Discarding obvious HST observations pointed at bright nearby targets, such as moving solar system objects, bright Galactic SF regions or star-clusters, and nearby galaxies including their SF-regions, Carleton et al. (2022) used the remaining images to measure the object-free sky-SB versus wavelength and Ecliptic or Galactic coordinates. These HST sky-SB measurements are on an *absolute flux scale* with a long term precision of $\lesssim$2.7–4%, including all known sources of systematics for WFC3/IR, ACS/WFC, WFC3/UVIS and WFPC2, respectively. When compared to the best available Zodiacal model of Kelsall et al. (1998), Carleton et al. (2022) find a residual amount of Diffuse Light (DL) that is present in the HST images of the order of $\lesssim$29–40 nW m^{-2} sr^{-1} at 1.25–1.6 μm wavelength. O'Brien et al. (2023) expanded this work down to the WFC3/UVIS wavelengths of 0.2 μm, and found residual Diffuse Light levels $\lesssim$22–32 nW m^{-2} sr^{-1} at 1.25–1.6 μm, with stricter target filtering, and more precise HST zeropoint monitoring over decades with an accuracy of $\lesssim$1–3%. While also monitoring the thermal properties of the HST and WFC3 hardware components over 15 years, McIntyre et al. (2024) made detailed estimates of the WFC3/IR thermal dark signal levels, and further refined these HST Diffuse Light estimates in excess of the best values for the Zodiacal, IGL and the Diffuse Galactic Light (DGL) to be less than $\lesssim$21–32 nW m^{-2} sr^{-1}, now also with lower bounds of $\gtrsim$2–20 nW m^{-2} sr^{-1} at

1.25–1.6 μm wavelength respectively. These are the best estimates available for the Diffuse Light that HST consistently sees in between its detected discrete objects such as stars and galaxies from LEO.

These HST Diffuse Light results provide some very interesting perspective when viewed in the context of recent work with the LORRI camera on board the New Horizons (NH) spacecraft from beyond Pluto's orbit, which initially found Diffuse Light levels at 0.4–0.9 μm of $\sim$8–14 nW m^{-2} sr^{-1} at 0.6 μm (Lauer et al. 2021, 2022; Symons et al. 2023), which were later revised down to $\lesssim$3.0 nW m^{-2} sr^{-1} after observing more NH fields in this manner (Postman et al. 2024). In summary, while HST from LEO at 1 AU sees Diffuse Light signals of order $\lesssim$20–25 nW m^{-2} sr^{-1}, New Horizons at distance $\gtrsim$40 AU from the Sun — where the Zodiacal Light is certainly very dim if not undetectable — detects less than 3 nW m^{-2} sr^{-1} at similar wavelengths. In conclusion, the best Zodiacal Light models, which have been around for over 25 years (Kelsall et al. 1998), may be missing a very dim (spherical or spheroidal) level of Diffuse Light in the inner solar system that HST clearly detects. McIntyre et al. (2024) suggest that this extra diffuse light might come from icy dust particles left in the inner solar system by comets on their way around the sun, and efforts are currently underway to update the Zodiacal Light models accordingly. In any case, thanks to the combined work of HST and New Horizons — it seems now unlikely that this Diffuse Light comes predominantly from cosmological distances. Very low levels of Diffuse Light from outside the solar system may come from dim tidal tails between galaxies, or from Inter Halo or Inter Group Light in galaxy groups (see *e.g.*, Postman et al. 2024; Windhorst et al. 2022, 2023, for further discussions). **This Diffuse Light work with HST can be done thanks to its unique property of having zeropoints stable to (well) within $\lesssim$1–2% over the decades and well calibrated HST images taken over many decades. This Archival HST work is the most difficult at its UV–blue wavelengths — also in terms of the Zodiacal foreground modeling — and continued HST monitoring of the sky-SB at 0.2–0.9 μm wavelengths would add very valuable and tighter constraints to any Diffuse Light that may come from outside the solar system and possibly have a cosmological origin (*e.g.*, O'Brien et al. 2023).**

5. ONGOING AND FUTURE UV-OPTICAL WORK: WHERE IS HST HEADING NOW JWST IS WORKING?

In this section, we will discuss ongoing and future UV-optical work, focusing on where is HST heading now JWST is working. We will focus on the topics of the UV-optical variability of weak AGN in the context of the process of galaxy assembly, and long-term HST UV-optical monitoring of SNe Ia as standard candles.

5.1. *UV-Optical Variability of Weak AGN in the context of Galaxy Assembly*

Super Massive Black Holes are ubiquitous at the centers of local galaxies (Kormendy & Richstone 1995) and their masses are possibly the most important factor in determining the evolution of galaxies and their unique properties (*e.g.*, Silk & Rees 1998; Granato et al. 2004). This is evidenced by well-established scaling relations between the SMBH mass and properties of the host spheroids, such as stellar velocity dispersion (*e.g.*, Gebhardt et al. 2000; Merritt & Ferrarese 2001) and stellar mass (*e.g.*, Magorrian et al. 1998; Marconi & Hunt 2003). Tracing both evolution of SMBHs and the build-up of stellar mass over most of cosmic time is key to gaining a quantitative and chronological understanding of galaxy assembly and evolution.

Traditional methods of identifying AGN, such as X-ray or mid-infrared emissions, sometimes miss those that are faint or lack strong emissions (e.g., Boutsia et al. 2009; Sarajedini et al. 2003; Pouliasis et al. 2019; Lyu et al. 2022). Variability offers a unique window into detecting AGN. It is caused by an unsteady inflow of matter onto a host galaxy's SMBH accretion disk, which can vary due to disruptions, changes in the flow rate, turbulence, and temperature changes (Shakura & Sunyaev 1976; Ulrich et al. 1997; Kawaguchi & Mineshige 1999). Variability is particularly useful for identifying faint AGN, as studies find that fainter AGN tend to show more significant changes in brightness (Hook et al. 1994; Trevese et al. 1994; Cristiani et al. 1997; Giveon et al. 1999; Vanden Berk et al. 2004; Wilhite et al. 2008). Past HST studies have highlighted the potential of variability to uncover unobscured faint, variable AGN (e.g., Cohen et al. 2006; Morokuma et al. 2008; Villforth et al. 2010; Sarajedini et al. 2003, 2011; Zhong et al. 2022). Nonetheless, further work is needed to pinpoint the true effect weak variable AGN have on their host galaxies. Key unanswered questions include the distribution of variable AGN across cosmic time, the influence of variability on star-formation, whether variability can be observed in dusty galaxies that have enough outflows (along narrow cones), or the active lifetimes of variable AGN.

HST remains essential to observe the extremely faint rest-frame UV-optical signals that can be associated with unobscured time-variable AGN. Previous studies (Cohen et al. 2006; Sarajedini et al. 2003; Villforth et al. 2010;

Pouliasis et al. 2019; Zhong et al. 2022; O'Brien et al. 2024; Hayes et al. 2024) were able to identify variability as faint as ∼0.2 mag. For AGN largely unobscured by dust from the surrounding torus or galaxy — *i.e.*, those AGN whose accretion disk and its outflow cone shine mostly in our direction — detection of AGN variability in the rest-frame UV–optical is optimal, as variability has been shown to increase at the shorter wavelengths (*e.g.*, Paltani & Courvoisier 1994; di Clemente et al. 1996; Helfand et al. 2001). Hence, HST is *the* platform of choice to monitor weak AGN variability at $z \lesssim 2$ — where half of the cosmic AGN growth takes place (Fig. 1 & 7e) — and constrain their accretion rates. (For SMBH accretion disks more significantly obscured by dust, JWST is needed of course to identify the central AGN component, see *e.g.*, Ortiz et al. 2024). HST's resolution is essential to separate the rest-frame UV accretion disks of AGN from the host galaxy for resolved objects. HST's F606W filter provides the optimal combination of depth (as faint as AB∼28.0 mag) and increased variability. Longer wavelengths would cause the variability to appear over longer time-scales, while shorter wavelength filters have relatively lower sensitivity.

Fig. 9 shows an example of a recently proposed time-domain survey strategy that optimally leverages the use of both of HST's wide field imagers to repeatedly map a large area (∼200 arcmin^2) on the sky over the course of 3 HST cycles to secure a deep (AB$\lesssim$28 mag) 7–15 epoch time-series enabling discovery and characterization of both AGN (actively accreting SMBHs) and different types of transients over most of cosmic history (B. Smith & R. Jansen; private communication). Note how this layout does *not* require 180° flips in orientation of HST to provide the desired areal overlap of the ACS/WFC and WFC3/UVIS observations, and is thus feasible in reduced gyro mode. A number of known transients and variable sources from O'Brien et al. (2024), resulting from only small areas of 2-epoch overlap of ACS/WFC F606W observations in this field (the NEP Time-Domain Field Jansen & Windhorst 2018) is overlaid. Also shown are locations of sources of synergistic interest to other NASA missions (*e.g.*, Chandra, NuSTAR; Zhao et al. 2021, 2024) and ground-based facilities (*e.g.*, J-VLA, JCMT Hyun et al. 2023; Willner et al. 2023), where HST's UV–optical wavelengths provide a crucial link in the energy range between X-ray and radio for transient phenomena at intermediate and high redshifts. Other such survey fields are available in the NEP, *e.g.*, the IRAC Dark Field (IDF; Yan et al. 2023a). Fig. 1 also shows the cosmic AGN space density (Wolf et al. 2003), cosmic star-formation rate (Madau & Dickinson 2014), and SNe Type Ia (Frohmaier et al. 2019) and IIn (Cold & Hjorth 2023) rates vs. redshift. The peaks of these curves are seen to coincide approximately at $z \simeq 2$ ("cosmic noon"; see Fig. 1), suggesting an underlying relation causing the co-evolution of SMBH masses and galaxy (spheroid) stellar mass build-up. **Detecting and monitoring the rest-frame UV–blue radiation from unobscured hot stellar populations and unobscured accretion disks (weak AGN) is *the* unique capability of HST. With its unique resolution and sensitivity in the optical, long term monitoring with HST is the only observatory that can capture the faintest SNe and AGN variability signals in significant numbers at this crucial epoch in cosmic time at $z \lesssim 2$. Such survey fields scattered through the North Ecliptic Pole and elsewhere in the HST CVZ will be most precious targets for upcoming long-term HST monitoring campaigns to study weak AGN variability and high redshift SNe.**

5.2. *Long-Term HST UV-Optical Monitoring of SNe Ia as Standard Candles*

A major issue in using luminosity distances from SNe Ia is a possible intrinsic evolution of SN properties with the age and metallicity of the progenitor stars. The existing samples SNe Ia have shown residual correlations with host-galaxy properties, perhaps reflecting uncorrected age, metallicity, and dust differences among progenitors (*e.g.*, Mannucci et al. 2006; Kelly et al. 2010; Sullivan et al. 2010; Lampeitl et al. 2010; Childress et al. 2013; Rigault et al. 2013, 2015; Uddin et al. 2017; Roman et al. 2018; Rigault et al. 2020; Smith et al. 2020b; Nicolas et al. 2021; Brout & Scolnic 2021; Kelsey et al. 2021; Briday et al. 2022). Lower metallicities at higher redshift implies that the progenitor stars are less likely to lose mass through stellar winds. As a result, the average mass of the white dwarfs at high-z is expected to be larger than their $z \simeq 0$ counterparts. These systematic differences are expected to be the most significant at redshifts $z \simeq 1.5$–3.0 (*e.g.*, Riess & Livio 2006, see also Fig. 1 here). Optical HST imaging is perfectly suited to identify these explosions and the progenitor host galaxy in great detail, enabling the study of environmental effects on SNe Ia's and their progenitor white dwarfs. Evidence for a dependence of SNe Ia luminosities on progenitor metallicities, age, or other environmental effects would have profound implications on the current cosmological paradigm.

Non-rotating stars with helium core masses of ∼65–130 $M_\odot$ within massive 140–260 $M_\odot$ stellar envelopes are expected to lead to the production of electron–positron pairs before oxygen ignition, causing rapid contraction and the ignition of explosive oxygen burning. This leads to an energetic thermonuclear runaway known as a pair-instability SN (PISN), which ejects large amounts of heavy elements into the surrounding medium, leaving no remnant behind. PISNe

require their progenitors to have an extremely low metallicity (*e.g.*, Langer et al. 2007), since massive stars with higher metallicities produce strong stellar winds, resulting in significant mass loss that prevents the formation of a massive helium core. The first generation of massive stars are predicted to enrich the early interstellar medium through PISNe (*e.g.*, Heger & Woosley 2002). Confirming the existence of PISNe would be a critical confirmation of our understanding of stellar evolution theory (Langer et al. 2007). **Wide-band, optical long-term monitoring in HST continuous viewing zones would provide, for the first time, the ability to identify a sample of these elusive PISNe from their unique light curves alone.**

5.3. *HST Studies of Individual Stars at Cosmological Distances via Cluster Caustic Transits*

One of the most stunning — and rather unforeseen — discoveries of HST was the detection of individual stars at cosmological distances through cluster caustic transits. This possibility was first predicted by Miralda-Escude (1991), where a star at cosmological distances would temporarily undergo very high gravitational magnification when the foreground cluster moves its caustic surface across the very small angular diameter of the star at the source redshift. Magnifications of many factors of 1000–10,000 are in principle possible, as the magnification factor scales as $\mu \propto (10\text{–}20)/\sqrt{d}$, where d is the distance of the star (in arcsec) to the caustic. This could temporarily boost the brightness of a very compact object by $\mu \gtrsim$7.5–10 mag on timescales of months, since stars at cosmological distances will have angular diameters of order $\sim 10^{-11}$–10^{-10} arcsec, and the clusters can have lateral velocities in the cosmic flow of $v \simeq$1000 km s^{-1} (Kelly et al. 2018; Windhorst et al. 2018). Microlensing by compact objects (*e.g.*, faint stars, brown dwarfs) in the Inter Cluster Medium (ICM) can dilute the amplitude of the lensed caustic-transit signal somewhat, but also spread it out over a correspondingly longer timescale (*e.g.*, Diego et al. 2018). Cluster microlensing by itself yields interesting constraints to the Dark Matter (DM) nature and content of the lensing cluster's ICM (*e.g.*, Diego et al. 2024a,b; Broadhurst et al. 2024; Pozo et al. 2024). The probability of such caustic transits happening depends of the surface brightness (SB) of the underlying stellar population (*i.e.*, a small galaxy or star cluster) that provides the lucky lensed stars, the transverse peculiar velocity of the foreground lensing cluster, the effective caustic length, as well as the temperature, luminosity and radius (or angular diameter at that distance) of the lensed stars (see, *e.g.*, Windhorst et al. 2018, for detailed calculations for stars at z$\gtrsim$7). While originally though to be the exclusive domain of detections by JWST at z$\gtrsim$6–7, HST has in fact detected a number of caustic transits in the last decade.

In 2018, Kelly et al. (2018) and Rodney et al. (2018) used HST to identify the caustic transiting star "Icarus" at z$\simeq$1.49, which they identified as a 20,000 K B-star. In 2022, Welch et al. (2022a) used HST to find a lucky star ("Earendel" or the Morning Star) at redshift z$\simeq$6.2 behind lensing cluster WHL0137-08 at z=0.566. Earendel was detected at the very redshift limit where HST can do this kind of work. Indeed, JWST was needed to get an accurate SED of this star (Welch et al. 2022b), which showed that it may in fact be a double star with component temperatures of ∼9,000 and 34,000 K each. Since then, a number of caustic transits have been found with HST at lower redshifts, where the HST blue performance is essential for the discovery as well as it proper interpretation. Further examples of high redshift caustic transits have been found with JWST, *e.g.*, at z$\simeq$1 behind MACS0416 (*e.g.*, Yan et al. 2023b, see Fig. 8 here) and at z=2.091 also behind MACS0416 (*e.g.*, Diego et al. 2023) — in both cases using the very deep HST Frontier Field (HFF) images as first epoch and separate red from blue stars — and at z=4.78 (*e.g.*, Meena et al. 2023; Furtak et al. 2024).

Most of these stellar caustic transits discovered so far are not single stars, but have the SEDs or spectra of double stars. This is expected, because most luminous stars in our own Galaxy are part of binary systems at the top of the stellar luminosity function (LF). As far as we can tell, many of these double stars are combinations of cooler red stars and hotter blue stars — also expected for binary stars in our own Galaxy. The caustic transiting sample available thus far consists by selection of luminous Blue Super Giants (BSGs) best detected by HST at intermediate redshifts, and of Red Super Giants (RSGs) best detected with JWST. At the higher redshifts, JWST is the more efficient telescope to detect caustic transit for the RSGs in such stellar binaries, while HST is the more efficient telescope to detect the BSGs. Indeed, some of caustic transiting binaries would not have been properly identified without HST imaging and photometry at bluer wavelengths than what JWST can do.

Finally, a stunning number of 40 caustic transits (!) was discovered including essential HST data in the Dragon's arc at z=0.725 behind the cluster Abell 370 at z=0.37 (*e.g.*, Fudamoto et al. 2024; Broadhurst et al. 2024). While JWST provided the second epoch for this unbelievable result, HST provided the essential first-epoch deep imaging, as well as the leverage to separate the BSGs from the RSGs identified by JWST. **These results are fundamental in that**

they are starting to allow us to directly constrain the (top-end of the) Initial Mass Function (IMF) at cosmological distances by just counting individual magnified stars.

6. KEEPING HST'S UNIQUE CAPABILITIES ALIVE IN THE CONTEXT OF FUTURE SPACE MISSIONS

It is also critical to keep HST's unique capabilities alive for as long as possible in the context of future space missions. Here, we mention:

• (1) The ESA Euclid mission (*e.g.*, Euclid Collaboration et al. 2024), launched in July 2023, is a 1.2 m telescope with a Wide Field Imager (WFI) that is covering ∼14,000 deg^2 in 4 broad-band filters spanning the 0.6–2μm wavelength range to AB$\lesssim$26.7 mag. WFI has one visual filter that spans a very wide range of 5500–9000 Å designed for weak lensing. Euclid also provides spectroscopic redshifts for brighter objects using two near-IR grisms.

• (2) The Nancy Grace Roman Space Telescope (*e.g.*, Akeson et al. 2019, "Roman"), scheduled for launch in May 2027, is a 2.4 m telescope with a Wide Field Imager. Its community surveys will map many 100's of deg^2 to AB$\lesssim$28–29 mag in 6 filters between 0.6–2μm, although only its bluest filter (R062) overlaps "HST-unique" parameter space, in that JWST does not have an equivalent filter.

Both space telescopes aim to constrain the cosmological parameters through a combination of Baryon Acoustic Oscillations (BAO), weak lensing, and/or high redshift Supernovae. Both Euclid and Roman thus lack the large suite of HST-unique filters between 0.2–0.6 μm wavelength, so they cannot replace HST. Moreover, in the narrow wavelength where they do overlap with HST, the detector sampling (0.″298/pixel for Euclid; Euclid Collaboration et al. (2024), and 0.″11/pixel for Roman; Akeson et al. (2019)), and hence the effective angular resolution attained by either mission is ∼2.8–7.5× worse than HST's WFC3/UVIS (which has 0.″039/pixel; *e.g.*, Windhorst et al. 2011), so that their sensitivity per unit time to the faintest point sources ∼7.8–57× worse than HST's.

• (3) The Chinese Space Station Telescope (CSST or "Xuntian") is a 2 m telescope intended to be launched later in the 2020's, and will be near the Chinese Space Station to enable regular servicing (*e.g.*, Gong et al. 2019; Cao et al. 2022). The aim for CSST is to cover ∼17,500 deg^2 in 7 broad- and 9 medium-band filters between 0.25–1.0 μm to AB$\lesssim$25–26 mag (*e.g.*, Gong et al. 2019, their Table 1) with science goals like weak lensing and galaxy clustering. Xuntian will have PSF-widths of ∼0.″20–0.″24 FWHM (Gong et al. 2019), so that the CSST PSF will cover about a ∼25× larger area than the HST UV–optical PSF FWHM^2 values, respectively. Hence, the CSST will *not* enable the high resolution studies like those illustrated in Fig. 3–7 here for the fainter and smallest galaxies. A significant fraction of faint galaxies would simply remain unresolved at 0.″24 resolution to AB$\lesssim$27 mag in the UV-optical (see *e.g.*, Fig. 10a of Windhorst et al. (2011) and Fig. 6a of Windhorst et al. (2023)). In addition, it is not clear that the US space community would have access to the CSST. Also, one must bear in mind that UV imaging poses very demanding requirements from the hardware, which HST was designed to have from the outset, such as: (1) the ability to mitigate Charge Transfer Efficiency (CTE) degradation of the CCDs over time caused by the steady intense Cosmic Ray (CR) flux in LEO (see *e.g.*, Appendix C of Smith et al. 2018, for a discussion). This effect is quite significant in the UV, especially after a few years in orbit, and can be mitigated by post-flashing each exposure at the appropriate level (see, *e.g.*, Smith et al. 2020a, 2024, and references therein); (2) have UV filters with redleaks (in the red wings of the filter curves) that are $\lesssim 10^{-5}$ of the filter peak transmission (see, *e.g.*, Fig. 1b and Appendix B of Smith et al. 2018), to enable reliable LyC detections for reionization studies; and (3) minimize outgassing from the nearby space station or servicing vehicle that could significantly reduce the UV reflectivity of the optics. In summary, the CSST cannot serve as a replacement of HST, especially not replace its superb UV-optical performance at fainter fluxes, but if it works as advertised, it will be a valuable UV–optical complement to the Euclid and Roman space telescopes over wider fields, but to brighter flux levels than what HST can do. **NASA can simply not afford to dismantle HST because we may some day have CSST.**

7. CONCLUSIONS

We conclude this tale of the two essential and complementary telescopes as following. HST is essential to image the unobscured cosmic star-formation and the growth of weak AGN accretion disks in the last 10 billion years since z$\lesssim$2, and JWST is essential to image the start and ramp-up of cosmic star-formation and AGN growth in the first few billion

years. In similar vein HST is essential to measure and identify caustic transits — especially their BSG components — at z$\lesssim$2, while JWST is essential to identify their RSGs components, and push the caustic transit search all the way into the epoch of reionization (z$\gtrsim$7).

In summary, using full cost accounting, the HST flagship mission will have costed over 20 B$ since the early 1970's (including all 6 Shuttle missions), while the JWST flagship mission will have costed over 10 B$ since the mid 1990's. Therefore, to get full return on our investment in JWST, HST will need to remain playing its unique and strong complementary role to JWST for as long as possible.

It is also essential to keep Hubble's mission funding strong, not only to keep the HST-unique instruments running for as long as possible, but also to maintain viable grant funding for HST observers, which will train students in HST work that prepares them well to work on future space missions.

8. WHAT UNIQUE HST IMAGING CAPABILITIES MUST BE PRESERVED AS MUCH AS POSSIBLE?

The following are unique HST imaging capabilities that must be preserved at the highest priority for the "Galaxies" science category:

• WFC3/UVIS: For its fully HST-unique imaging in the UV and blue optical wavelengths (0.2-0.8μm) that complements JWST NIRCam (0.9–5 μm), as explained above in § 1–6;

• ACS/WFC: High-resolution, low-background optical polarimetry and spectropolarimetry are entirely unique to ACS in space or on the ground; there are various unique science cases for polarimetry including weak AGN;

• ACS/WFC: The ACS ramp filters are regularly used, are a unique HST capability, and are crucial to certain investigations (see *e.g.*, the recent CXO press release). The ACS linear ramp capability cannot be replaced by the limited selection of WFC3 UVIS narrow-band filters;

• ACS/WFC: The parallel use of WFC3/IR and ACS/WFC as in, *e.g.*, the HFFs, CANDELS, UVCANDELS (and many other projects) offers the unique ability to efficiently map out larger areas than can be done with JWST. This mapping speed is very important and it is more efficient than JWST due to slewing overheads. Prime/parallel observing with WFC3 continues to be in *very heavy* demand by the user community: a sizable fraction of the $\gtrsim$1000 ACS orbits allocated in Cycle 32 are TAC approved ACS-WFC3 prime/parallel combinations. Both sky-coverage and filter coverage are boosted by this mode of operation, in ways that make certain types of observing programs uniquely affordable to the TAC. **If ACS/WFC can no longer trail WFC3/UVIS in parallel (or vice versa), HST will lose a full factor 3.44 in survey efficiency: namely a factor of 1.56 for the ACS/WFC3 FOV-ratio, and another factor of 1.56 in the ACS/WFC3 F606W throughput-ratio, *i.e.*, having ACS/WFC+WFC3/UVIS together produces (1+2.44)$\times$ the survey speed of just having WFC3/UVIS alone!**;

• ACS/WFC: There have been arguments put forward that Reduced Gyro Mode (RGM) critically hampers ACS-WFC3 prime/parallel observing, and that Charge Transfer Efficiency (CTE) degradation disadvantages ACS/WFC more than WFC3/UVIS. These arguments are not necessarily correct: WFC3 UVIS also has significant CTE in its UV-optical filters, and especially affects its UV filters, more so than ACS (see *e.g.*, Smith et al. 2018, 2020a, 2024, for detailed discussions). CTE degradation can be mitigated by properly post-flashing the ACS and WFC3 exposures, but comes at the expense of somewhat larger image noise, which can be mitigated through longer integrations;

• The ACS detectors, and especially ACS/WFC, are among the most stable on HST (see *e.g.*, Calamida et al. 2022; O'Brien et al. 2023, for detailed discussions);

• WFC3/IR has some unique high-resolution grism like G102 that JWST does not have. The WFC3/IR also has a very high-speed mapping capability (*e.g.*, the DASH program) by reading its IR chip out in scanning mode while the telescope moves at the appropriate rate, resulting in very large near-IR areas covered that have served as finder surveys of rare bright objects worthy of JWST follow-up.

Acknowledgments: We dedicate this paper to the memory of Dr. John B. Hutchings, who during his lifetime was a inspiration to us, and a great advocate of using Hubble with its many UV capabilities. We are deeply indebted to the many thousands of people who made Hubble such a success during the last three decades, and to those many thousands who have been doing the same for JWST. We thank Professors Marcia Rieke and Daniel Eisenstein for helpful suggestions, and for the tremendous job that they, and their team, did in making NIRCam and the JADES survey happen. We thank Dr. Christopher Willmer for his help clarifying the effective HUDF exposure times in the

public JADES data. We acknowledge support from HST grants that enabled us to pursue our more recent Hubble work, such as HST-AR-13877, HST-AR-14591, HST-GO-15278, HST-GO-15647, HST-AR-15810, HST-GO-16252, HST-GO-16605, HST-GO-16621, and HST-GO-16793, provided by NASA through the Space Telescope Science Institute, which is operated by the Association of Universities for Research in Astronomy, Inc., under NASA contract NAS 5-26555. RAW, SHC, and RAJ further acknowledge support from NASA JWST Interdisciplinary Scientist grants NAG5-12460, NNX14AN10G and 80NSSC18K0200 from GSFC. We also acknowledge the indigenous peoples of Arizona, including the Akimel O'odham (Pima) and Pee Posh (Maricopa) Indian Communities, whose care and keeping of the land has enabled us to be at ASU's Tempe campus in the Salt River Valley, where much of our work was conducted.

REFERENCES

Adams, N. J., Conselice, C. J., Austin, D., et al. 2024, ApJ, 965, 169

Akeson, R., Armus, L., Bachelet, E., et al. 2019, arXiv e-prints, arXiv:1902.05569

Andrews, S. K., Driver, S. P., Davies, L. J. M., Lagos, C. d. P., & Robotham, A. S. G. 2018, MNRAS, 474, 898

Beckwith, S. V. W., Stiavelli, M., Koekemoer, A. M., et al. 2006, AJ, 132, 1729

Beichman, C. A., Rieke, M., Eisenstein, D., et al. 2012, in Society of Photo-Optical Instrumentation Engineers (SPIE) Conference Series, Vol. 8442, Space Telescopes and Instrumentation 2012: Optical, Infrared, and Millimeter Wave, ed. M. C. Clampin, G. G. Fazio, H. A. MacEwen, & J. Oschmann, Jacobus M., 84422N

Boutsia, K., Leibundgut, B., Trevese, D., & Vagnetti, F. 2009, A&A, 497, 81

Briday, M., Rigault, M., Graziani, R., et al. 2022, A&A, 657, A22

Broadhurst, T., Li, S. K., Alfred, A., et al. 2024, arXiv e-prints, arXiv:2405.19422

Brout, D., & Scolnic, D. 2021, ApJ, 909, 26

Calamida, A., Bajaj, V., Mack, J., et al. 2022, AJ, 164, 32

Cao, Y., Gong, Y., Zheng, Z.-Y., & Xu, C. 2022, Research in Astronomy and Astrophysics, 22, 025019

Carleton, T., Windhorst, R. A., O'Brien, R., et al. 2022, AJ, 164, 170

Childress, M., Aldering, G., Antilogus, P., et al. 2013, ApJ, 770, 108

Coe, D. 2015, Trilogy: FITS image conversion software, Astrophysics Source Code Library, record ascl:1508.009, , , ascl:1508.009

Cohen, S. H., Ryan, R. E., J., Straughn, A. N., et al. 2006, ApJ, 639, 731

Cold, C., & Hjorth, J. 2023, A&A, 670, A48

Conselice, C. J., Adams, N., Harvey, T., et al. 2024, arXiv e-prints, arXiv:2407.14973

Cristiani, S., Trentini, S., La Franca, F., & Andreani, P. 1997, A&A, 321, 123

di Clemente, A., Giallongo, E., Natali, G., Trevese, D., & Vagnetti, F. 1996, ApJ, 463, 466

Dickinson, M. 1995, in Galaxies in the Young Universe, ed. H. Hippelein, K. Meisenheimer, & H.-J. Röser, Vol. 463, 144

Dickinson, M., Dey, A., & Spinrad, H. 1995, in Galaxies in the Young Universe, ed. H. Hippelein, K. Meisenheimer, & H.-J. Röser, Vol. 463, 164

Diego, J. M., Kaiser, N., Broadhurst, T., et al. 2018, ApJ, 857, 25

Diego, J. M., Sun, B., Yan, H., et al. 2023, A&A, 679, A31

Diego, J. M., Amruth, A., Palencia, J. M., et al. 2024a, A&A, in press, arXiv:2406.08537

Diego, J. M., Kei Li, S., Amruth, A., et al. 2024b, A&A, 689, A167

Driver, S. P., Fernández-Soto, A., Couch, W. J., et al. 1998, ApJL, 496, L93

Driver, S. P., Windhorst, R. A., Ostrander, E. J., et al. 1995, ApJL, 449, L23

Driver, S. P., Andrews, S. K., Davies, L. J., et al. 2016, ApJ, 827, 108

Duncan, K., Conselice, C. J., Mundy, C., et al. 2019, ApJ, 876, 110

Eisenstein, D. J., Willott, C., Alberts, S., et al. 2023, arXiv e-prints, arXiv:2306.02465

Euclid Collaboration, Mellier, Y., & et al., A. 2024, arXiv e-prints, arXiv:2405.13491

Freedman, W. L., & Madore, B. F. 2023, JCAP, 2023, 050

Freedman, W. L., Madore, B. F., Jang, I. S., et al. 2024, arXiv e-prints, arXiv:2408.06153

Frohmaier, C., Sullivan, M., Nugent, P. E., et al. 2019, MNRAS, 486, 2308

Fudamoto, Y., Sun, F., Diego, J. M., et al. 2024, Nat. Astron., arXiv:2404.08045

Furtak, L. J., Meena, A. K., Zackrisson, E., et al. 2024, MNRAS, 527, L7

Gardner, J. P., Mather, J. C., Abbott, R., & et al. 2023, PASP, 135, 068001

Gardner, J. P., Mather, J. C., Clampin, M., et al. 2006, SSRv, 123, 485
Gebhardt, K., Bender, R., Bower, G., et al. 2000, ApJL, 539, L13
Giavalisco, M., Ferguson, H. C., Koekemoer, A. M., et al. 2004, ApJL, 600, L93
Giveon, U., Maoz, D., Kaspi, S., Netzer, H., & Smith, P. S. 1999, MNRAS, 306, 637
Gong, Y., Liu, X., Cao, Y., et al. 2019, ApJ, 883, 203
Granato, G. L., De Zotti, G., Silva, L., Bressan, A., & Danese, L. 2004, ApJ, 600, 580
Griffiths, R. E., Casertano, S., Ratnatunga, K. U., et al. 1994, ApJL, 435, L19
Grogin, N. A., Kocevski, D. D., Faber, S. M., et al. 2011, ApJS, 197, 35
Hayes, M. J., Tan, J. C., Ellis, R. S., et al. 2024, ApJL, 971, L16
Heger, A., & Woosley, S. E. 2002, ApJ, 567, 532
Helfand, D. J., Stone, R. P. S., Willman, B., et al. 2001, AJ, 121, 1872
Hook, I. M., McMahon, R. G., Boyle, B. J., & Irwin, M. J. 1994, MNRAS, 268, 305
Hyun, M., Im, M., Smail, I. R., et al. 2023, ApJS, 264, 19
Illingworth, G. D., Magee, D., Oesch, P. A., et al. 2013, ApJS, 209, 6
Jansen, R. A., & Windhorst, R. A. 2018, PASP, 130, 124001
Kartaltepe, J. S., Sanders, D. B., Scoville, N. Z., et al. 2007, ApJS, 172, 320
Kawaguchi, T., & Mineshige, S. 1999, in Activity in Galaxies and Related Phenomena, ed. Y. Terzian, E. Khachikian, & D. Weedman, Vol. 194, 356
Kelly, P. L., Hicken, M., Burke, D. L., Mandel, K. S., & Kirshner, R. P. 2010, ApJ, 715, 743
Kelly, P. L., Diego, J. M., Rodney, S., et al. 2018, Nature Astronomy, 2, 334
Kelsall, T., Weiland, J. L., Franz, B. A., et al. 1998, ApJ, 508, 44
Kelsey, L., Sullivan, M., Smith, M., et al. 2021, MNRAS, 501, 4861
Koekemoer, A. M., Faber, S. M., Ferguson, H. C., et al. 2011, ApJS, 197, 36
Koekemoer, A. M., Ellis, R. S., McLure, R. J., et al. 2013, ApJS, 209, 3
Kormendy, J., & Ho, L. C. 2013, ARA&A, 51, 511
Kormendy, J., & Richstone, D. 1995, ARA&A, 33, 581
Koushan, S., Driver, S. P., Bellstedt, S., et al. 2021, MNRAS, 503, 2033
Lampeitl, H., Smith, M., Nichol, R. C., et al. 2010, ApJ, 722, 566
Langer, N., Norman, C. A., de Koter, A., et al. 2007, A&A, 475, L19
Lauer, T. R., Postman, M., Weaver, H. A., et al. 2021, ApJ, 906, 77
Lauer, T. R., Postman, M., Spencer, J. R., et al. 2022, ApJL, 927, L8
Lilly, S. J., Le Fevre, O., Hammer, F., & Crampton, D. 1996, ApJL, 460, L1
Lyu, J., Alberts, S., Rieke, G. H., & Rujopakarn, W. 2022, ApJ, 941, 191
Madau, P., & Dickinson, M. 2014, ARA&A, 52, 415
Madau, P., Giallongo, E., Grazian, A., & Haardt, F. 2024, ApJ, 971, 75
Magorrian, J., Tremaine, S., Richstone, D., et al. 1998, AJ, 115, 2285
Mannucci, F., Della Valle, M., & Panagia, N. 2006, MNRAS, 370, 773
Marconi, A., & Hunt, L. K. 2003, ApJL, 589, L21
McIntyre, I. A., Carleton, T., O'Brien, R., et al. 2024, arXiv e-prints, arXiv:2407.12290
Meena, A. K., Zitrin, A., Jiménez-Teja, Y., et al. 2023, ApJL, 944, L6
Merritt, D., & Ferrarese, L. 2001, ApJ, 547, 140
Miralda-Escude, J. 1991, ApJ, 379, 94
Morokuma, T., Doi, M., Yasuda, N., et al. 2008, ApJ, 676, 163
Naidu, R. P., Oesch, P. A., Reddy, N., et al. 2017, ApJ, 847, 12
Nicolas, N., Rigault, M., Copin, Y., et al. 2021, A&A, 649, A74
O'Brien, R., Carleton, T., Windhorst, R. A., et al. 2023, AJ, 165, 237
O'Brien, R., Jansen, R. A., Grogin, N. A., et al. 2024, ApJS, 272, 19
Oesch, P. A., Montes, M., Reddy, N., et al. 2018, ApJS, 237, 12
Ortiz, Rafael, I., Windhorst, R. A., Cohen, S. H., et al. 2024, ApJ, in press, arXiv:2404.10709
Paltani, S., & Courvoisier, T. J. L. 1994, A&A, 291, 74
Pascarelle, S. M., Windhorst, R. A., Driver, S. P., Ostrander, E. J., & Keel, W. C. 1996a, ApJL, 456, L21
Pascarelle, S. M., Windhorst, R. A., Keel, W. C., & Odewahn, S. C. 1996b, Nature, 383, 45
Postman, M., Lauer, T. R., Parker, J. W., et al. 2024, ApJ, 972, 95
Pouliasis, E., Georgantopoulos, I., Bonanos, A. Z., et al. 2019, MNRAS, 487, 4285
Pozo, A., Broadhurst, T., Emami, R., et al. 2024, arXiv e-prints, arXiv:2407.16339

Rafelski, M., Teplitz, H. I., Gardner, J. P., et al. 2015, AJ, 150, 31
Rieke, M. J., Kelly, D., & Horner, S. 2005, in Society of Photo-Optical Instrumentation Engineers (SPIE) Conference Series, Vol. 5904, Cryogenic Optical Systems and Instruments XI, ed. J. B. Heaney & L. G. Burriesci, 1–8
Rieke, M. J., Robertson, B., Tacchella, S., et al. 2023a, ApJS, 269, 16
Rieke, M. J., Kelly, D. M., Misselt, K., et al. 2023b, PASP, 135, 028001
Riess, A. G., & Livio, M. 2006, ApJ, 648, 884
Riess, A. G., Scolnic, D., Anand, G. S., et al. 2024, arXiv e-prints, arXiv:2408.11770
Rigault, M., Copin, Y., Aldering, G., et al. 2013, A&A, 560, A66
Rigault, M., Aldering, G., Kowalski, M., et al. 2015, ApJ, 802, 20
Rigault, M., Brinnel, V., Aldering, G., et al. 2020, A&A, 644, A176
Rodney, S. A., Balestra, I., Bradac, M., et al. 2018, Nature Astronomy, 2, 324
Roman, M., Hardin, D., Betoule, M., et al. 2018, A&A, 615, A68
Sarajedini, V. L., Gilliland, R. L., & Kasm, C. 2003, ApJ, 599, 173
Sarajedini, V. L., Koo, D. C., Klesman, A. J., et al. 2011, ApJ, 731, 97
Scoville, N., Aussel, H., Brusa, M., et al. 2007, ApJS, 172, 1
Shakura, N. I., & Sunyaev, R. A. 1976, MNRAS, 175, 613
Silk, J., & Rees, M. J. 1998, A&A, 331, L1
Smith, B. M., Windhorst, R. A., Jansen, R. A., et al. 2018, ApJ, 853, 191
Smith, B. M., Windhorst, R. A., Cohen, S. H., et al. 2020a, ApJ, 897, 41
Smith, B. M., Windhorst, R. A., Teplitz, H., et al. 2024, ApJ, 964, 73
Smith, M., Sullivan, M., Wiseman, P., et al. 2020b, MNRAS, 494, 4426
Smith, R. W., Hanle, P. A., Kargon, R. H., & Tatarewicz, J. N. 1993, The Space Telescope. A study of NASA, science, technology, and politics.
Soifer, B. T., Helou, G., & Werner, M. 2008, ARA&A, 46, 201
Sullivan, M., Conley, A., Howell, D. A., et al. 2010, MNRAS, 406, 782
Symons, T., Zemcov, M., Cooray, A., Lisse, C., & Poppe, A. R. 2023, ApJ, 945, 45
Teplitz, H. I., Rafelski, M., Kurczynski, P., et al. 2013, AJ, 146, 159
Thompson, R. I., Storrie-Lombardi, L. J., Weymann, R. J., et al. 1999, AJ, 117, 17
Trevese, D., Kron, R. G., Majewski, S. R., Bershady, M. A., & Koo, D. C. 1994, ApJ, 433, 494
Uddin, S. A., Mould, J., Lidman, C., Ruhlmann-Kleider, V., & Zhang, B. R. 2017, ApJ, 848, 56
Ulrich, M.-H., Maraschi, L., & Urry, C. M. 1997, ARA&A, 35, 445
Vanden Berk, D. E., Wilhite, B. C., Kron, R. G., et al. 2004, ApJ, 601, 692
Villforth, C., Koekemoer, A. M., & Grogin, N. A. 2010, ApJ, 723, 737
Wang, X., Teplitz, H. I., Smith, B. M., et al. 2023, arXiv e-prints, arXiv:2308.09064
Welch, B., Coe, D., Diego, J. M., et al. 2022a, Nature, 603, 815
Welch, B., Coe, D., Zackrisson, E., et al. 2022b, ApJL, 940, L1
Werner, M. W., Lowrance, P. J., Roellig, T., et al. 2022, Journal of Astronomical Telescopes, Instruments, and Systems, 8, 014002
Werner, M. W., Roellig, T. L., Low, F. J., et al. 2004, ApJS, 154, 1
Wilhite, B. C., Brunner, R. J., Grier, C. J., Schneider, D. P., & vanden Berk, D. E. 2008, MNRAS, 383, 1232
Williams, R. E., Blacker, B., Dickinson, M., et al. 1996, AJ, 112, 1335
Willner, S. P., Gim, H. B., Polletta, M. d. C., et al. 2023, ApJ, 958, 176
Windhorst, R. A., Hathi, N. P., Cohen, S. H., et al. 2008, Advances in Space Research, 41, 1965
Windhorst, R. A., Cohen, S. H., Hathi, N. P., et al. 2011, ApJS, 193, 27
Windhorst, R. A., Timmes, F. X., Wyithe, J. S. B., et al. 2018, ApJS, 234, 41
Windhorst, R. A., Carleton, T., O'Brien, R., et al. 2022, AJ, 164, 141
Windhorst, R. A., Cohen, S. H., Jansen, R. A., et al. 2023, AJ, 165, 13
Wolf, C., Wisotzki, L., Borch, A., et al. 2003, A&A, 408, 499
Yan, H., Cohen, S. H., Windhorst, R. A., et al. 2023a, ApJL, 942, L8
Yan, H., Ma, Z., Sun, B., et al. 2023b, ApJS, 269, 43
Zhao, X., Civano, F., Fornasini, F. M., et al. 2021, MNRAS, 508, 5176
Zhao, X., Civano, F., Willmer, C. N. A., et al. 2024, ApJ, 965, 188
Zhong, Y., Inoue, A. K., Yamanaka, S., & Yamada, T. 2022, ApJ, 925, 157

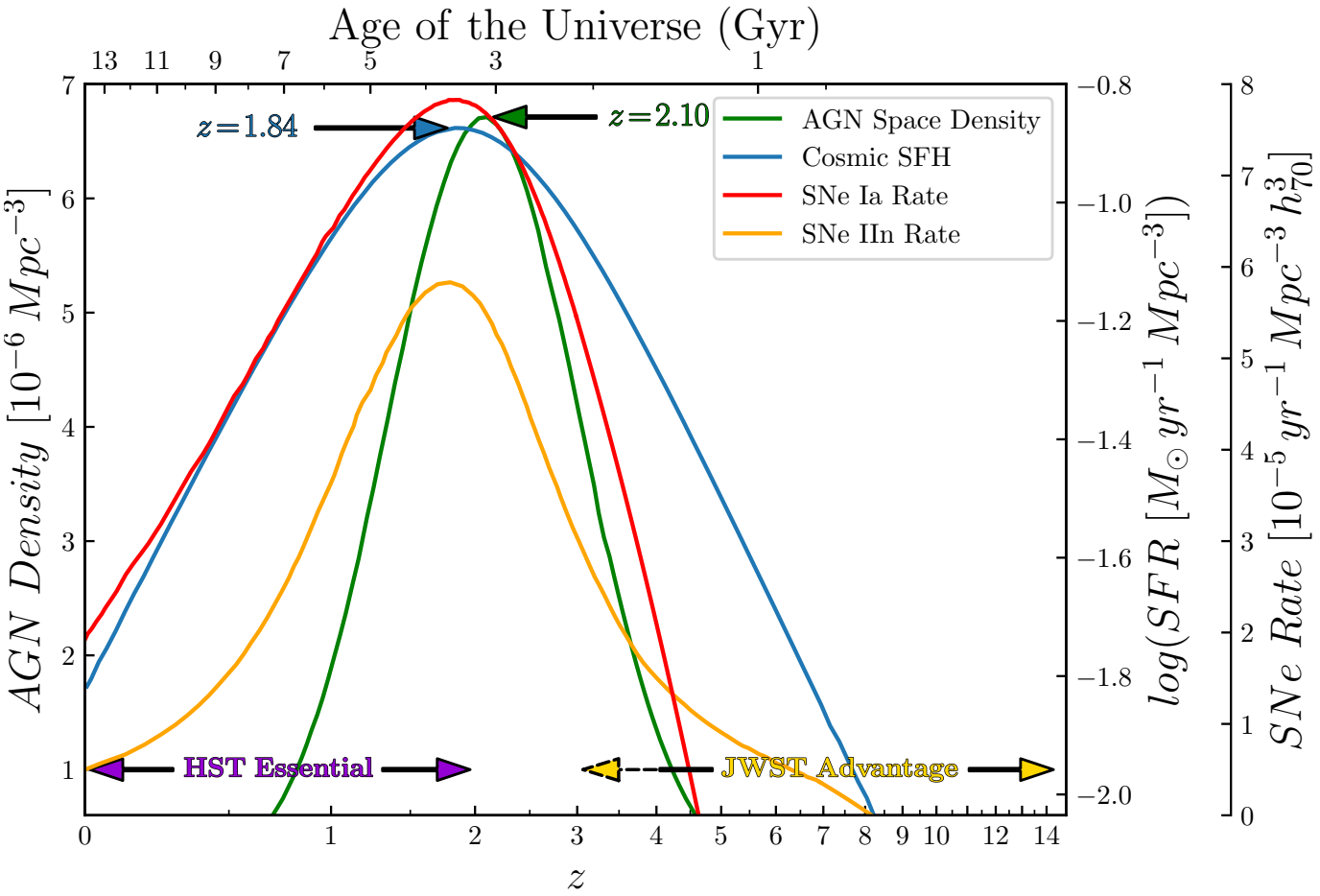

Figure 1. Cosmic AGN space density (Wolf et al. 2003, green), cosmic star-formation rate (Madau & Dickinson 2014, blue), and SNe Type Ia (Frohmaier et al. 2019, red) and IIn (Cold & Hjorth 2023, orange) rates vs. redshift. (The units of the three vertical scales are displayed at arbitrary normalization, so the four curves peak at similar amplitudes). The peaks of these curves are indicated and coincide approximately at redshift z≃2 ("cosmic noon"), suggesting an underlying relation causing the co-evolution of SMBH masses and galaxy (spheroid) stellar mass build-up. The Galaxy Assembly and SMBH epoch of the last 10 billion years at z$\lesssim$2, where the HST-unique UV-optical images are essential are indicated by the purple arrow, while the epoch of the first 2 billion years at z$\gtrsim$3 where JWST has its main advantage is indicated by the orange arrow. **Detecting and monitoring the rest-frame UV–blue radiation from unobscured hot stellar populations and accretion disks (weak AGN) is** *the* **unique capability of HST. With its unique resolution and sensitivity in the UV-optical, long term monitoring with HST is the only observatory that can capture the faintest SNe and AGN variability signals in the UV-optical in significant numbers at this crucial epoch in cosmic time.**

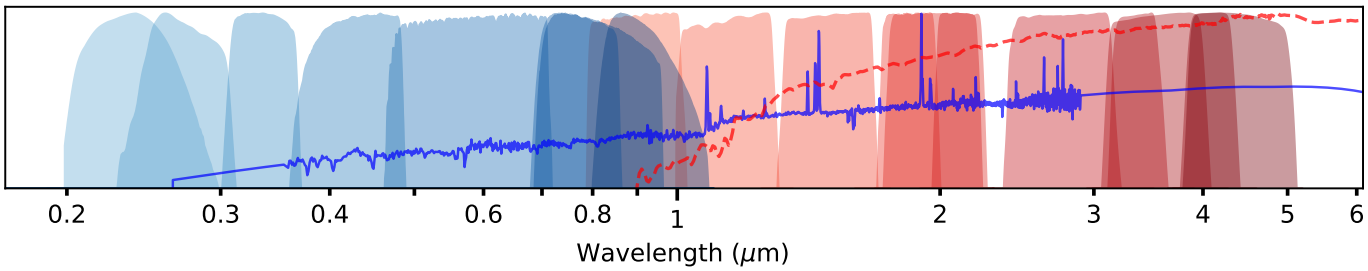

Figure 2. Throughput curves of the HST (blue) and JWST (red) filters to render the full complement of available HUDF data, with a star-forming (blue) and old (red) elliptical galaxy SED overlaid at the peak redshift z≃1.9 of the cosmic SFH (Fig. 1).

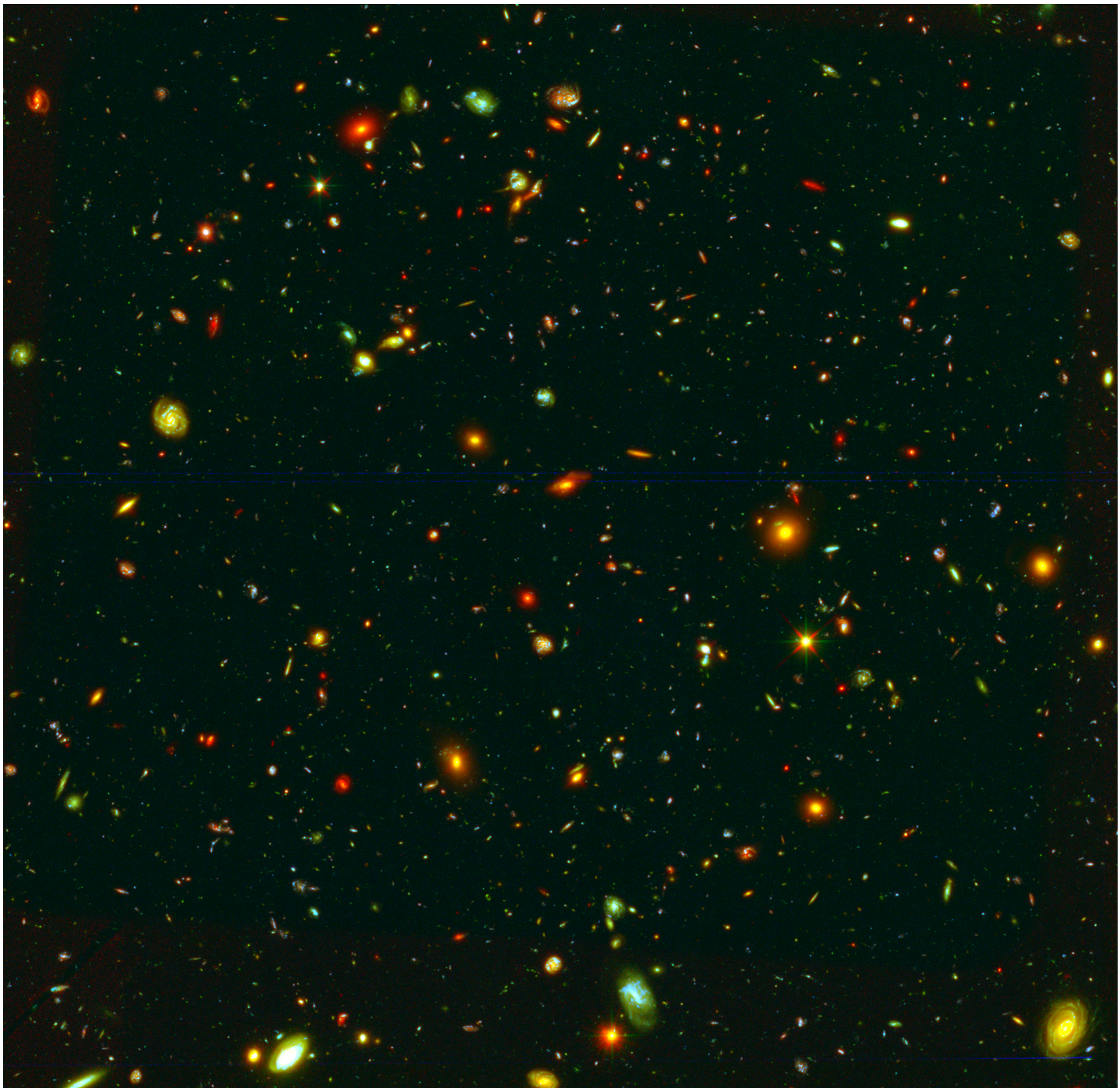

Figure 3. Full color image of the Hubble UltraDeep Field with 891 orbits (556.3 hours) of HST time in 12 HST filters: WFC3/UVIS F225W, F275W, and F336W and ACS/WFC F435 filters have been noise-weighted and rendered in blue, the ACS/WFC F606W, F775W, F814W and F850LP filters were noise-weighted and rendered in green, while the WFC3/IR filters F105W, F125W, F140W, and F160W were noise-weighted and rendered in red. (The bottom left corner was not covered by HST/WFC3, and so does not show the very reddest objects well). All HUDF images are shown at 0.″06/pixel, and are 2580×2510 in size with North at a PA of –47.5°. **Please highly magnify sections of these 4 color images (20 Mb each), and blink them to show the complementarity of the unique HST UV-optical and JWST near-IR imaging capabilities.**

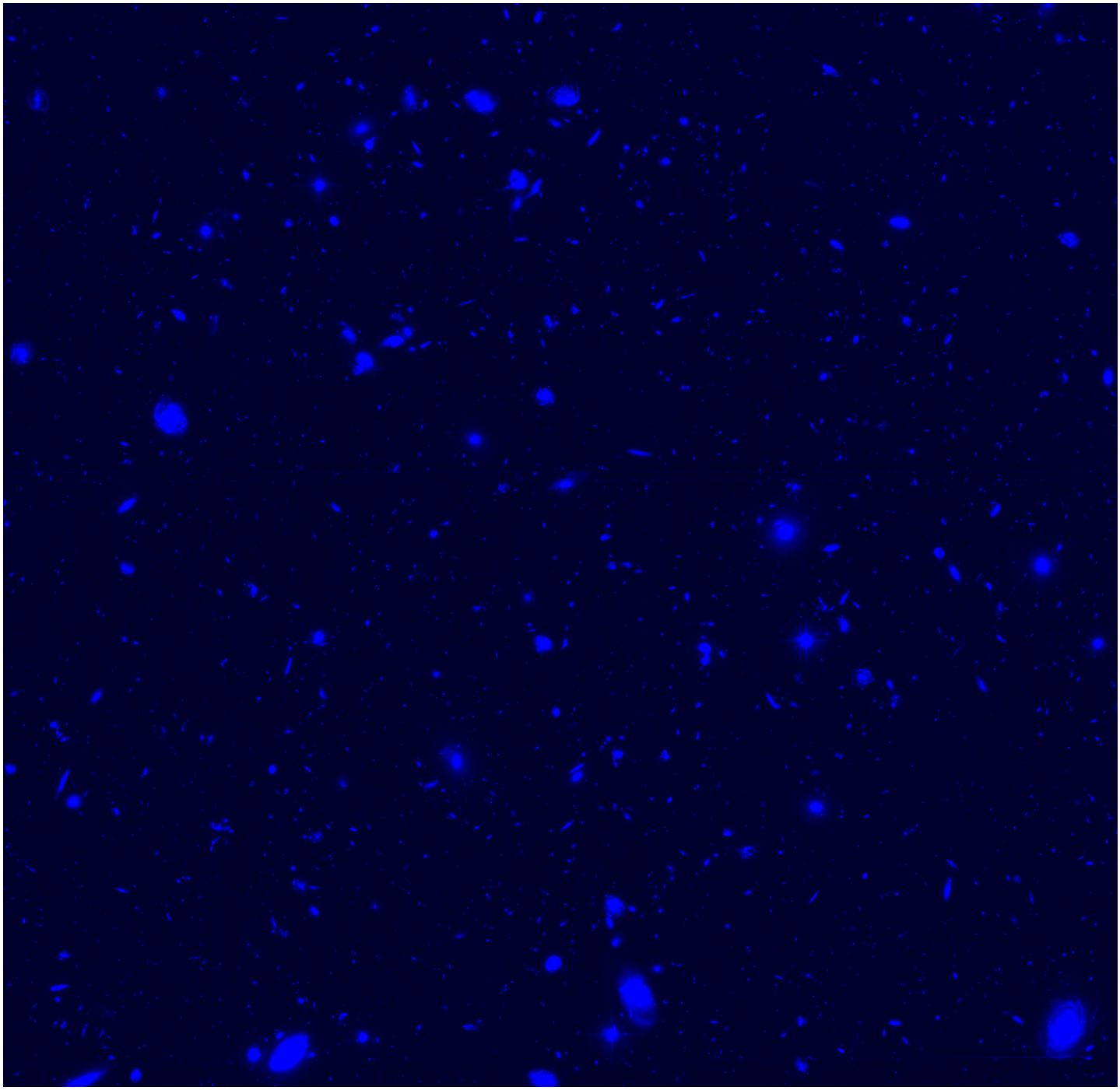

Figure 4. False color image of the Hubble UltraDeep Field in the 8 bluest *HST-unique* filters (WFC3/UVIS F225W, F275W, and F336W and ACS/WFC F435W, F606W, F775W, F814W and F850LP) from Fig. 3, but now all noise-weighted and rendered **only** in the blue channel. This demonstrates the HST-unique UV–blue photons from *recent star-formation* that represent the more recent cosmic SFH at z≃0–2 — *i.e.*, from the peak in the cosmic SFH and more recently — which JWST does not sample for the hottest stellar rest-frame wavelengths.

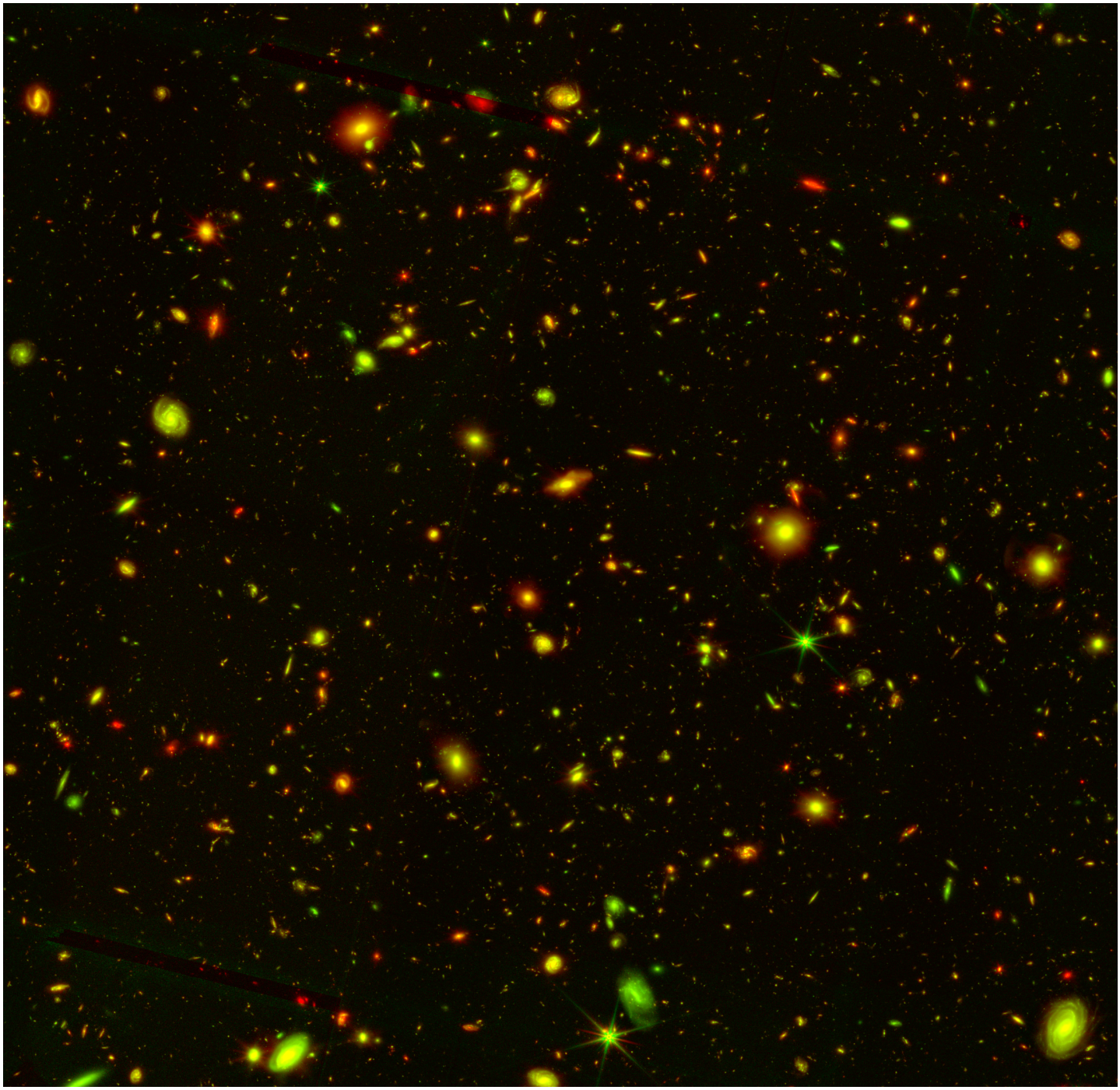

Figure 5. Color image of the publicly available 52.7 hour JWST NIRCam JADES images (Rieke et al. 2023a; Eisenstein et al. 2023) of the same HUDF area as covered by Hubble in Fig. 3–4. To best illustrate the JWST sensitivity to infrared objects — and mimic the colors closest to the what the human eye can see — all NIRCam filter images were noise-weighted and rendered in green (F090W, F115W, F150W, F182M, F200W, and F210M) or in red (F277W, F335M, F356W, F410M, and F444W). **The JWST NIRCam data alone sample the rest-frame optical part of the cosmic star-formation history at $z \lesssim 2$, and further into the rest-frame UV at $z \gtrsim 2$ (see Fig. 7e).**

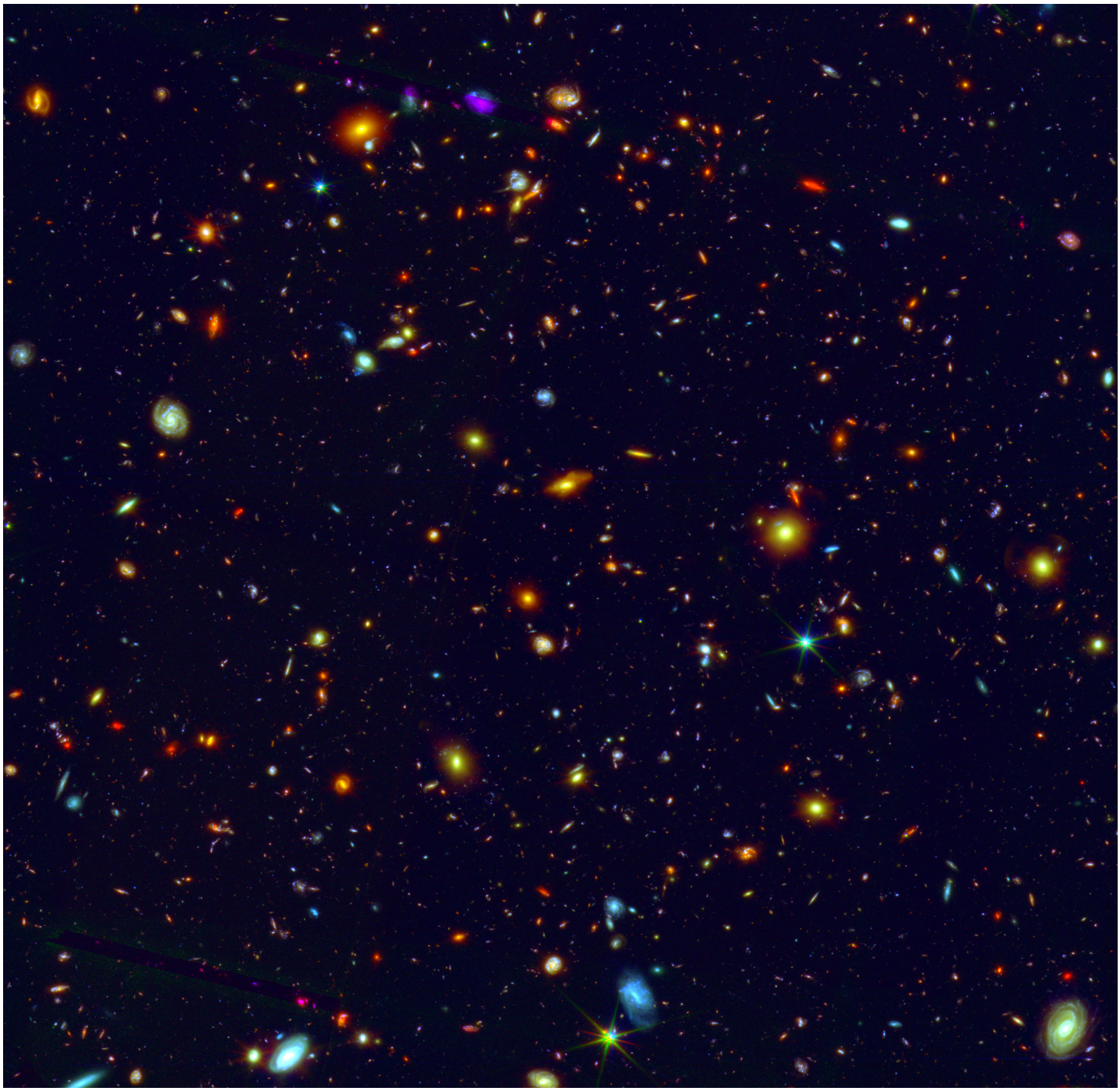

Figure 6. Full color image of the *combined* public 361.3 hour HST + 52.7 hour JWST data from Fig. 4–5 rendered in full panchromatic RGB. The 8 bluest *HST-unique* filters (WFC3/UVIS F225W, F275W, and F336W, ACS/WFC F435W, F606W, F775W, F814W and F850LP) were noise-weighted and rendered in blue, the JWST NIRCam SW filter images in green (F090W, F115W, F150W, F182M, F200W, F210M), and the JWST NIRCam LW filter images in red (F277W, F335M, F356W, F410M, F444W). **At 414 hours, this is the deepest combined HST+JWST color image available to date, and demonstrates the strong complementarity of HST to JWST: HST adds the unique unobscured restframe UV+blue that samples the more recent half of the CSFH in the last 10 billion years ($z \lesssim 2$), compared to the JWST restframe optical–near-IR that samples older and/or more dusty stellar populations, and very rare objects at $z \gtrsim 10$–13 seen in the first 300–500 Myr.**

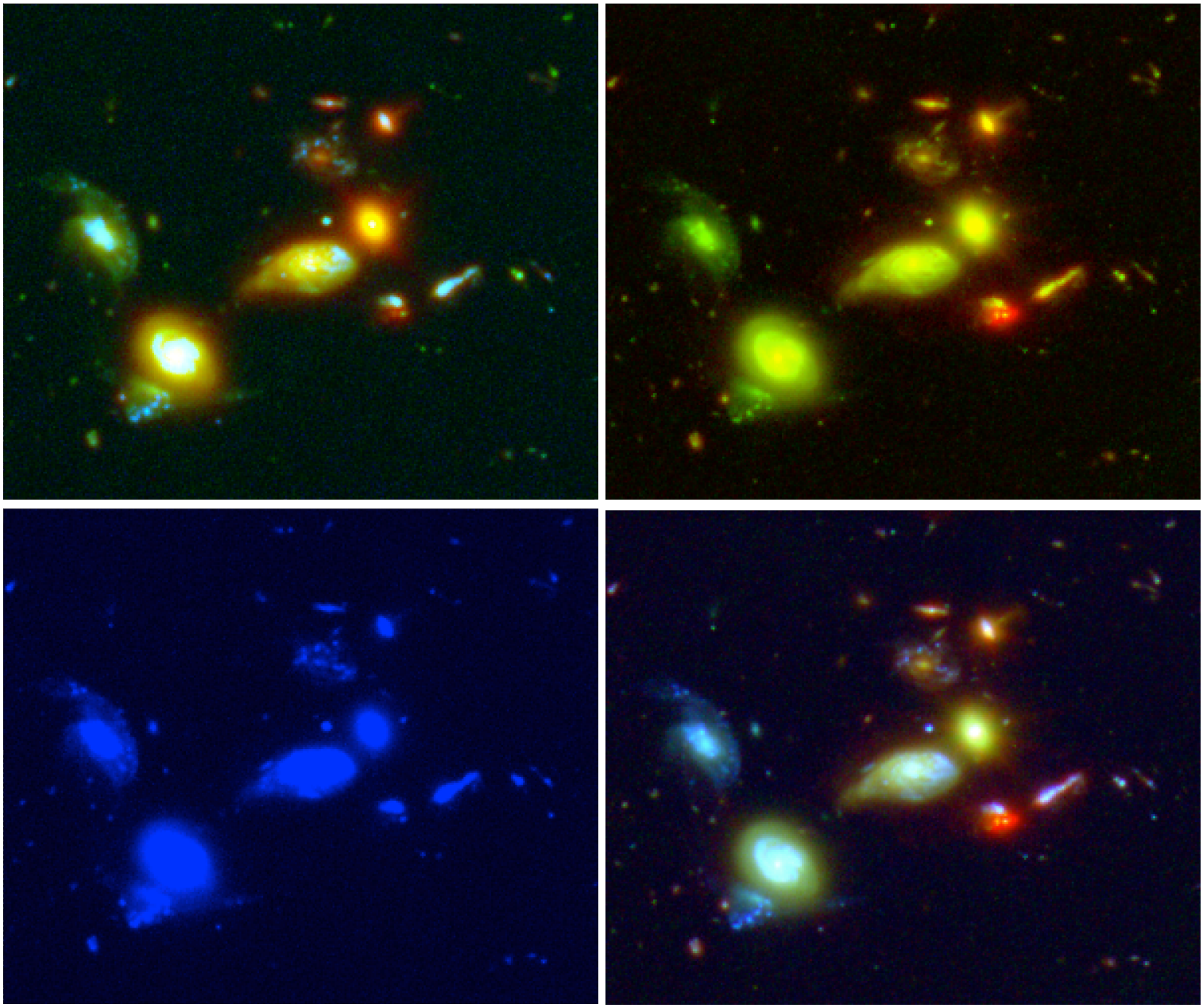

Figure 7. Enlargement of an area with a number of HUDF galaxies with a wide variety of morphologies and star-formation histories from Fig. 3–6, illustrating the power of combining 361.3 hours of HST UV-optical images with 52.7 hours of JWST NIRCam images. **7a. [Upper Left]:** Enlargement from Fig. 3: all 12 HST filters only rendered in RGB; **7b. [Lower Left]:** Enlargement from Fig. 4: 8 UV-optical HST filters in false color blue; **7c. [Upper Right]:** Enlargement from Fig. 5: 8 JWST NIRCam filters rendered in green and red only; **7d. [Lower Right]:** Enlargement from Fig. 6: best combination of Fig. 7b and 7c rendered in full panchromatic RGB. **7e. [Bottom]:** Same as Fig. 2 shown once more for clarity, to show the throughput curves of the HST (blue) and JWST (green and red) filters used to render the full complement of available HUDF data in 7d. A star-forming (blue) and an old (red) elliptical galaxy SED are overlaid at the peak redshift z≃1.9 of the cosmic SFH (Fig. 1).

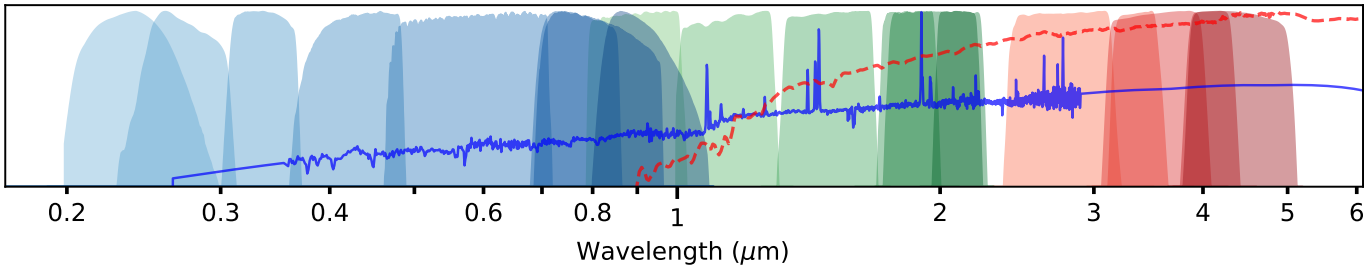

Figure 8. Color image of the *combined public 122-hour HST Frontier Field images with ACS/WFC plus the 3-epoch 22-hour JWST PEARLS NIRCam images* on galaxy cluster MACS0416 at redshift z=0.397. Like Fig. 6, this image perfectly illustrates the power of combining HST images in the restframe UV–blue with JWST images in the restframe optical–near-IR. This image was also featured on: https://www.nytimes.com/2023/12/19/science/christmas-stars-galaxies-webb-nasa.html?. Details on the science resulting from these very deep combined HST+JWST MACS0416 cluster images can be found in Diego et al. (2023) and Yan et al. (2023b).

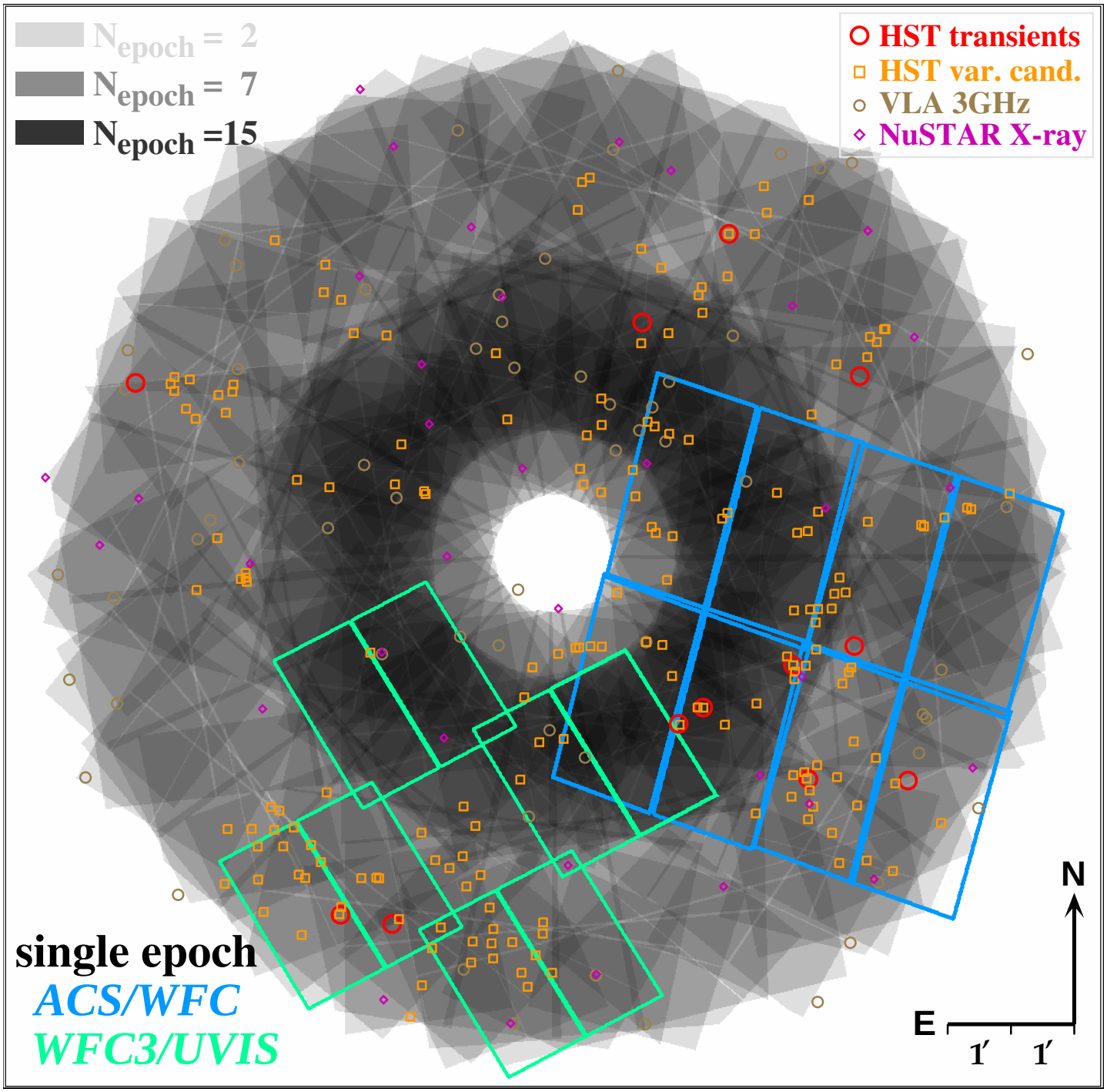

Figure 9. Example of a recently proposed time-domain survey strategy that optimally leverages the use of both of HST's wide field imagers to repeatedly map a large area (∼200 arcmin^2) on the sky over the course of 3 cycles to secure a deep (AB$\lesssim$28 mag) 7–15 epoch time-series enabling discovery and characterization of both AGN (actively accreting SMBHs) and different types of transients over most of cosmic history (B. Smith & R. Jansen; private communication). Note how this layout does *not* require 180° flips in orientation of HST to provide the desired areal overlap of the ACS/WFC and WFC3/UVIS observations, and is feasible in reduced gyro mode. A smattering of known transients and variable sources from O'Brien et al. (2024), resulting from small areas of 2-epoch overlap of ACS/WFC F606W observations in this field (the NEP Time-Domain Field; Jansen & Windhorst 2018) is overlaid. Also shown are locations of sources of synergistic interest to other NASA missions (Chandra, NuSTAR) and ground-based facilities (J-VLA, JCMT) where HST's UV–optical wavelengths provide a crucial link in the energy range between X-ray and radio for transient phenomena at intermediate and high redshifts. **Such HST-unique Time Domain surveys need to be continued with Hubble to complement these other NASA missions for as long as possible.**